Received: 4 November 2019 | Revised: 19 March 2020 | Accepted: 31 March 2020

DOI: 10.1002/glia.23835

GLIA

WILEY

RESEARCH ARTICLE

# The metabolic response to inflammation in astrocytes is regulated by nuclear factor-kappa B signaling

Josephine L. Robb | Nadia A. Hammad | Paul G. Weightman Potter | John K. Chilton | Craig Beall | Kate L. J. Ellacott

Institute of Biomedical and Clinical Science, University of Exeter Medical School, Exeter, UK

**Correspondence**
Kate L. J. Ellacott, Institute of Biomedical and Clinical Science, University of Exeter Medical School, Exeter, UK.
Email: k.ellacott@exeter.ac.uk

**Present address**
John K. Chilton, Peninsula Medical School, University of Plymouth, Plymouth, UK

**Funding information**
Diabetes UK, Grant/Award Number: 13/0004647; European Foundation for the Study of Diabetes; Medical Research Council, Grant/Award Number: MR/N012763/1; University of Exeter Medical School

## Abstract

Inflammation and metabolism are intrinsically linked with inflammatory stimuli inducing metabolic changes in cells and, in turn, metabolic capacity determining cellular inflammatory responses. Although well characterized in peripheral immune cells there is comparatively less known about these "immunometabolic" responses in astrocytes. In this study, we tested the hypothesis that the astrocytic inflammatory response driven by nuclear factor-kappa B (NF-κB) signaling is dependent on glycolytic metabolism. Using mouse primary cortical astrocyte cultures, we assessed changes in cellular metabolism after exposure to lipopolysaccharide (LPS), with cytokine ELISAs and immunoblotting being used to measure inflammatory responses. Results indicate temporally distinct metabolic adaptations to pro-inflammatory stimulation in astrocytes: 3 hr LPS treatment increased glycolysis but did not alter mitochondrial metabolism, while following 24 hr of LPS treatment we observed increased oxidative phosphorylation, and decreased glycolytic capacity and glucose uptake, partly due to reduced glucose transporter 1 expression. Inhibition of NF-κB signaling with the IKK-beta inhibitor TPCA-1 prevented the LPS induced changes to glycolysis and oxidative phosphorylation. Furthermore, TPCA-1 treatment altered both glycolysis and oxidative phosphorylation independently from inflammatory stimulation, indicating a role for NF-κB signaling in regulation of basal metabolism in astrocytes. Inhibition of glycolysis with 2-deoxyglucose significantly attenuated LPS-induced cytokine release and NF-κB phosphorylation, indicating that intact glycolysis is required for the full inflammatory response to LPS. Together our data indicate that astrocytes display immunometabolic responses to acute LPS stimulation which may represent a potential therapeutic target for neuroinflammatory disorders.

KEYWORDS

astrocyte, glycolysis, inflammation, metabolism, nuclear factor-kappa B

## 1 | BACKGROUND

In peripheral immune cells of the myeloid and lymphoid lineage, inflammatory stimuli differentially modulate metabolic pathways including glycolysis and oxidative phosphorylation, with the full immune response being dependent on the activity of these processes (O'Neill, Kishton, & Rathmell, 2016; Russell, Huang, & VanderVen, 2019). This bidirectional relationship between immune and metabolic function has become known as "immunometabolism." Immunometabolism is emerging as a therapeutic target for disease, leading to the repurposing of pharmaceuticals targeting cellular metabolism (e.g., Metformin) for conditions including cancers (Singer, Cheng, Kreutz, Ho, & Siska, 2018), Alzheimer's disease (Campbell et al., 2018; Koenig et al., 2017), and autoimmune diseases such as multiple sclerosis and lupus (Norata et al., 2015). Anti-inflammatory drugs are also being investigated to treat metabolic diseases including Type-2 diabetes and obesity (Goldfine et al., 2008; Goldfine et al., 2010; Lee, Wollam, & Olefsky, 2018). Despite the therapeutic potential of this approach, there is less understanding of whether the same immunometabolic changes are also seen in the central nervous system (CNS), most notably in astrocytes.

Astrocytes are important for the maintenance of the CNS microenvironment and are key regulators of neuronal activity and behavior, resulting in physiological changes in the whole organism (Liddelow et al., 2017). Astrocytes become inflamed in vivo in response to a broad range of inflammatory conditions, including metabolic stress or infection, and undergo a series of morphological and functional adaptations termed astrogliosis (Sofroniew & Vinters, 2010; Zamanian et al., 2012). Preventing inflammation in astrocytes through inhibition of the nuclear factor-kappa B (NF-κB) signaling pathway can alter the pathophysiological response to disease. For example, inhibition of NF-κB activity in glial-fibrillary acidic protein (GFAP) expressing astrocytes promotes functional recovery of spinal cord injury in mice, resulting in reduced glial scarring and increased locomotor activity (Brambilla et al., 2005). Additionally, in the context of metabolic disease, inhibition of astrocyte NF-κB signaling in the mouse, by deleting IκB kinase β from GFAP expressing cells, improves glucose tolerance and reduces obesity by promoting energy expenditure (Douglass, Dorfman, Fasnacht, Shaffer, & Thaler, 2017).

Some existing evidence already links inflammation with changes in cellular metabolism in astrocytes. In aging mice, increased NF-κB activity in astrocytes correlates with elevated aerobic metabolism (Jiang & Cadenas, 2014). Furthermore, in vitro studies in mouse primary astrocytes demonstrate that treatment with inflammatory cytokines increases their glucose uptake, reduces intracellular glycogen stores, and increases flux through the tricarboxylic acid (TCA) cycle and pentose phosphate pathway (Bélanger, Allaman, & Magistretti, 2011; Gavillet, Allaman, & Magistretti, 2008). In a related study, Meares et al. showed that decreasing substrate availability to astrocytes in vitro, by limiting glucose and pyruvate, reduces interferon-gamma-induced inflammatory responses (Meares, Qin, Liu, Holdbrooks, & Benveniste, 2013). The anti-inflammatory effect of reduced glucose or pyruvate availability was replicated by pharmacological activation of the cellular energy sensor AMP-activated protein kinase (AMPK) (Meares et al., 2013). Exposure to nitric oxide, which can be an inflammatory factor in high concentrations (Sharma, Al-Omran, & Parvathy, 2007), also enhances the activity of signaling pathways which regulate glycolysis in astrocytes: hypoxia inducible factor 1α and AMPK (Almeida, Moncada, & Bolaños, 2004; Brix, Mesters, Pellerin, & Jöhren, 2012). Together these data suggest that astrocytes rely on glycolysis to achieve full inflammatory activation, but to our knowledge, this important question has never been directly examined.

We tested the hypothesis that the astrocytic inflammatory response driven by NF-κB signaling is dependent on glycolytic metabolism. The impact of inflammation on energy metabolism in astrocytes was investigated, including an examination of whether NF-κB signaling plays a role in the regulation of astrocyte metabolism during inflammation. Further understanding of the role of astrocyte metabolism in the inflammatory response may open the opportunity for new therapies for CNS disease.

## 2 | METHODS

### 2.1 | Reagents

Unless otherwise stated, all reagents were purchased from Sigma-Aldrich (part of Merck, UK) or ThermoFisher Scientific (UK).

### 2.2 | Animals and ethics

All animal studies were conducted in accordance with the UK Animals in Scientific Procedures Act 1986 (ASPA) and study plans were approved by the institutional Animal Welfare and Ethical Review Body at the University of Exeter. Mouse pups (postnatal Days 1–5) from breeding pairs of C57BL6/J mice (Charles River, UK) were used to produce cultures of primary astrocytes from the cortex; offspring of both sexes were used. Mice were group housed on a 12:12 light–dark cycle at 22 ± 2°C, with unlimited access to standard laboratory rodent diet (EURodent diet [5LF2], LabDiet, UK) and water.

### 2.3 | Primary astrocyte isolation and general cell culture

Mouse primary cortical astrocytes (CRTAS) were isolated using the method described by Schildge et al. (Schildge, Bohrer, Beck, & Schachtrup, 2013). Immunocytochemistry confirmed that mature cultures contained >99% GFAP-immunoreactive glial cells (supplementary Figure S1). As previously described (Vlachaki Walker et al., 2017), cultures were maintained in Dulbecco's Modified Eagle's Media (DMEM) containing 25 mM glucose and supplemented with 10% vol/vol fetal bovine serum ([FBS] Seralabs; UK), 200 U/ml penicillin–streptomycin and 8 mM L-glutamine. Cultures were maintained in a humidified incubator at 37°C with 5% $CO_2$. Prior to experimentation cells were seeded on poly-L-lysine (PLL; 4 μg/ml) coated plasticware at an appropriate density. Then, 24 hr prior to experimentation cells

were maintained in DMEM (Gibco; UK) supplemented with 10% vol/vol FBS, 200 U/ml penicillin–streptomycin, 8 mM L-glutamine and 7.5 mM glucose. On the day of experimentation, cells were cultured in serum free DMEM (Gibco; UK) containing 2.5 mM glucose.

## 2.4 | Cell treatments

Lipopolysaccharide (LPS; *Escherichia coli* O26:B6) was conjugated to 0.17 mM fatty acid and endotoxin free bovine serum albumin (BSA [Roche]) in 150 mM NaCl for 1 hr prior to treatment of cells. BSA was adjusted to pH 7.4 at 37°C with 1 N NaOH. BSA conjugated LPS or BSA vehicle were diluted 1:10 into DMEM to give a final concentration of 1 μg/ml LPS and 0.017 mM BSA. Where used, TPCA-1 (1 μM; Tocris [UK]; IKK-β inhibitor) was diluted in 0.1% vol/vol DMSO vehicle 2 hr prior to additional treatments. 2-deoxyglucose (2-DG; 10 mM; 0.1% vol/vol $H_2O$) was applied 1 hr prior to additional treatments, when used.

## 2.5 | Immunocytochemistry and culture purity

For immunocytochemical staining, CRTAS were plated on sterile PLL coated 13 mm diameter glass coverslips at a density of $1 \times 10^5$ cells/coverslip. After treatment, cells were fixed with 4% wt/vol paraformaldehyde for 30 min at 37°C and permeabilized for staining by treatment with lysine block (PBS, 0.02% vol/vol Triton-X100, 2% wt/vol lysine) for 15 min. Purity of the CRTAS cultures was confirmed using mouse anti-GFAP (1:1,000; Millipore; UK; #MAB360) and goat anti-IBA1 (1:1,000; Abcam; UK; #ab5076) immunoreactivity. Both primary and secondary antibodies were diluted in lysine block. Fixed and permeabilized cells were incubated with each primary antibody overnight (~18 hr) at 4°C, sequentially. After incubation with GFAP primary antibody, coverslips were incubated with fluorescent secondary donkey anti-mouse Alexafluor488 (1:500; Invitrogen; UK; #A-21202) for 1 hr at room temperature. After incubation with IBA1 antibody overnight, fixed cells were incubated with fluorescent secondary donkey anti-goat Alexafluor594 (1:500; Invitrogen; UK; #A-11058) for 1 hr at room temperature. Both between and after antibody incubations, fixed cells were washed three times for 5 min with 1X PBS to remove unbound antibody. Nuclei were stained with DAPI (0.01 mg/ml). Coverslips were mounted in Fluoroshield Mounting Medium (Abcam) and allowed to dry prior to imaging using wide-field microscopy (DM4000B-M; 10x/0.30; Leica; UK). FIJI Cell Counter plugin (Fiji Is Just ImageJ; (Schindelin et al., 2012; Schneider, Rasband, & Eliceiri, 2012)) was used to manually count nuclei associated with GFAP or IBA-1 staining.

## 2.6 | Cell viability assay

Cells were seeded at a density of $3.5 \times 10^5$ cells/well in six well plates. After 24 hr of treatment (described above in Section 2.4) cells were dissociated with 0.05% trypsin–EDTA and transferred to flow cytometry tubes where trypsin was neutralized with fluorescence activated cell sorting (FACS) buffer (2% vol/vol FBS in 1X PBS). Cells were centrifuged at 100*g* for 5 min and the supernatant was aspirated. Cells were resuspended in FACS buffer and stained with propidium iodide (2 μg/ml), which is taken into cells with disrupted membranes, for 10 min at 4°C. Uptake of dye was determined using flow cytometry, with increased uptake representing cell death (BD Accuri C6; BD Systems; 488 nm; 633/22 nm). Gating used is shown in supplementary Figure S2a. Region of interest P1 in Plot 2 was used to select events classified as dead cells.

## 2.7 | Immunoblotting

Cells were plated at a density of $4.5 \times 10^5$ cells per 60 mm diameter dish. After treatment, cells were washed with 1X PBS to remove excess BSA. Cells were lysed and protein isolated with modified RIPA buffer (supplementary methods S1) and centrifugation at $1.3 \times 10^4 g$. Protein content was estimated using the Bradford method according to the manufacturer's instructions (BioRad; UK). Proteins were separated on a 12% vol/vol acrylamide gel using SDS-PAGE and transferred to nitrocellulose membranes. Precision plus protein Dual color standards (BioRad) were run on all gels and used to estimate protein size. Membranes were blocked for 1 hr in Odyssey Blocking Buffer (Tris-buffered saline [TBS]) (Licor; UK). Antibodies against proteins of interest were made up in 2.5% wt/vol milk powder or 2.5% wt/vol BSA in 1X TBS with 0.1% Tween (TBS-T) as detailed in supplementary methods S2 and incubated with the membranes overnight at 4°C. GAPDH expression was used as a loading control. Antibodies against GAPDH were incubated with membranes for 1 hr at room temperature (see supplementary methods S2 for further details). Expression of total NF-κB was estimated by stripping (1X Re-Blot Plus Strong Solution; Millipore), blocking and reprobing the same membranes used to assess phosphorylated NF-κB expression. Between antibody binding steps, blots were washed three times for 5 min with TBS-T. Bound antibody was detected with species specific fluorescent antibodies, incubated with membranes for 1 hr at room temperature (see supplementary methods S2 for further details). Protein was visualized using the Li-Cor Odyssey scanner. Fluorescence from detected protein was estimated with Image Studio software (V5.2; Licor). For NF-κB immunoblots, expression of phosphorylated NF-κB (normalized to GAPDH) was represented as a ratio of phosphorylated NF-κB (normalized to GAPDH):total NF-κB (normalized to GAPDH). Data are shown as fold change from the mean of control groups.

## 2.8 | Media cytokine concentrations

Cells were plated at a density of $4.5 \times 10^5$ cells per 60 mm diameter dish. Media was collected from cells after treatment and cytokine concentrations determined using DuoSet ELISAs (BioTechne; UK) against mouse TNF-α, IL-6, and IL-10 as per the manufacturer's instructions.

Cytokine concentrations were normalized to protein content, collected and estimated using the Bradford method (BioRad) as described above.

## 2.9 | Metabolic analyses

The metabolic rate of cells was determined by measuring the extracellular acidification rate (ECAR) as a measure of glycolysis, and oxygen consumption rate (OCR) as a measure of mitochondrial function using the Seahorse Metabolic Bioanalyzer XF$^e$96 (Agilent; UK). The day before treatment cells were plated in 96 well Agilent Seahorse Culture plates (Agilent) at $4 \times 10^4$ cells per well in supplemented DMEM (10% vol/vol FBS, 200 U/ml penicillin–streptomycin, 8 mM L-glutamine, and 7.5 mM glucose). After treatment, and 1 hr prior to experimentation, media was replaced with Seahorse XF DMEM medium (pH 7.4; Agilent) supplemented with either L-glutamine (2 mM; Glycolytic Stress Test) or L-glutamine (2 mM), glucose (2.5 mM), and sodium pyruvate (2.5 mM; Mito Stress Test). Cells were incubated for 1 hr at 37°C in a humidified non-$CO_2$ incubator. Glycolytic rate and oxidative metabolism were determined using Glycolytic Stress Tests and Mito Stress Tests, respectively, as per the manufacturer's instructions (Agilent).

### 2.9.1 | Glycolytic Stress Test

Cells were treated sequentially with glucose (10 mM), oligomycin (1 μM), and 2-DG (50 mM). All treatments were rehydrated in Seahorse XF DMEM medium (pH 7.4; Agilent) supplemented with 2 mM L-glutamine. Glycolytic rate describes the highest ECAR measurement after addition of glucose. Glycolytic capacity describes the maximum ECAR measurement after addition of oligomycin. Glycolytic reserve was calculated as the difference between glycolytic capacity and glycolytic rate.

### 2.9.2 | Mito Stress Test

Cells were treated sequentially with oligomycin (0.5 μM), carbonyl cyanide-4 (trifluoromethoxy) phenylhydrazone (FCCP; 1 μM), and rotenone with antimycin A (R/A; 0.5 μM). All treatments were rehydrated in Seahorse XF DMEM medium (pH 7.4; Agilent) supplemented with L-glutamine (2 mM), glucose (2.5 mM), and sodium pyruvate (2.5 mM). Basal respiration was calculated as OCR immediately prior to addition of oligomycin minus the lowest measurement after addition of R/A. ATP production was calculated as the difference between basal respiration and the lowest OCR measurement after addition of oligomycin. Proton leak was calculated as the difference between the lowest OCR measurement (after addition of oligomycin) and the lowest OCR measurement after addition of R/A. Maximal respiration was calculated as the maximum OCR measurement after FCCP addition, minus the lowest OCR measurement after R/A addition. Spare capacity was calculated as the difference between basal respiration and maximal respiration. Coupling efficiency was ATP production as a percentage of basal respiration.

## 2.10 | Glucose uptake, ATP, and glycogen content measurements

Glucose uptake was determined using Glucose Uptake-Glo kit (Promega) following the manufacturer's instructions. Cells were plated at $4 \times 10^4$ cells/well in 96 well plates. A total of 10 μM 2-DG was used, while omission of 2-DG used as a negative control. Luminescence was measured after 30 min incubation in detection reagent. Data are shown as fold change from the mean of contemporaneous control groups.

Intracellular ATP (iATP) concentrations were quantified using the ATPLite Two Step kit (PerkinElmer) following the manufacturer's instructions with modifications as previously described (Vlachaki Walker et al., 2017). Data are shown as fold change from the mean of contemporaneous control groups.

Glycogen content was measured using the Glycogen Assay Kit (Fluorometric; Cell Biolabs; UK). Cells were plated at $1 \times 10^6$ cells/dish in 100 mm Petri dishes. After treatment, cells were washed twice with PBS to remove exogenous glucose, collected in PBS and snap frozen. Cells were lysed through sonication at 4°C (LOW, 10 cycles, 10 on/10 off) and centrifuged at $1.3 \times 10^4 g$ for 20 min at 4°C. Supernatants were used for glycogen quantification. The assay was carried out following the manufacturer's instructions in black 96 well plates, and fluorescence was measured after 45 min incubation in the reaction mix. Values below detection are reported as zero.

All plate-based assays were quantified using a PheraStar plate reader (BMG).

## 2.11 | Mitochondrial membrane potential

Mitochondrial membrane potential was determined using tetramethylrhodamine ethyl ester (TMRE) dye uptake. Cells were plated in six well plates at $3.5 \times 10^5$ cells/well. After treatment (as appropriate), cells were dissociated using 0.05% trypsin–EDTA. Cells were transferred to flow cytometry tubes, and trypsin was neutralized with FACS buffer (2% vol/vol FBS in 1X PBS). Cells were centrifuged at 100*g* for 5 min and the supernatant was aspirated. Treatment for 15 min with FCCP (10 μM; 0.04% vol/vol DMSO vehicle in FACS buffer) at 37°C prior to TMRE dye uptake was used as a positive indicator of mitochondrial depolarization. Cells were resuspended and incubated with TMRE (100 nM) in 0.04% vol/vol DMSO vehicle and FACS buffer for 30 min at 37°C prior to centrifugation, aspiration of supernatant and resuspension in FACS buffer. Cellular fluorescence was measured using flow cytometry (BD Accuri C6; UK; 488 nm; 585/40 nm). Increased dye uptake correlates with increased mitochondrial polarization. An example of the gating used is

shown in supplementary methods S3. Events from P1 (Plot 1) were shown on Plot 3. Mean fluorescence of events counted in M2 (Plot 3) was taken as fluorescence of treatment group. M2 was determined as fluorescence intensity greater than the fluorescence intensity from the TMRE untreated control group. Data are shown as fold change from the mean of contemporaneous vehicle-treated control groups.

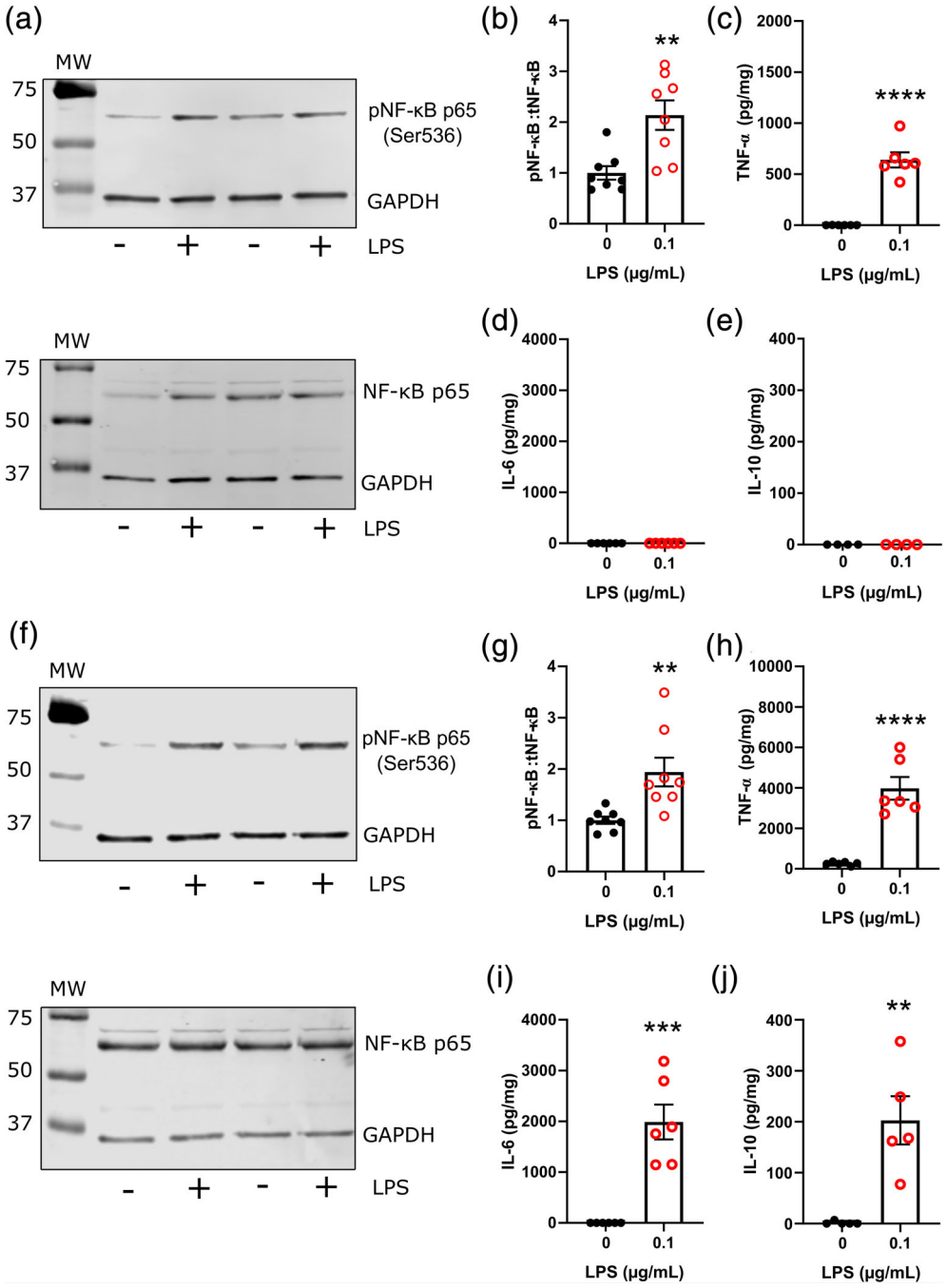


**FIGURE 1** Mouse primary cortical astrocytes displayed an inflammatory response to lipopolysaccharide (LPS). (a) Representative anti-phospho-nuclear factor-kappa B (NF-κB) p65 (Ser536) (top) and anti-total NF-κB p65 (bottom) immunoblot after 3 hr treatment with 0.1 μg/ml LPS with anti-GAPDH loading control. (b) Densitometric analysis of (a): anti-phospho-NF-κB p65 (Ser536) fluorescence as a ratio of anti-total NF-κB p65 normalized to anti-GAPDH fluorescence and represented as fold change in fluorescence from the mean of vehicle-treated controls ($n$ = 8). (c) Extracellular TNF-α concentration 3 hr after LPS treatment ($n$ = 6). (d) Extracellular IL-6 concentration 3 hr after LPS treatment ($n$ = 6). (e) Extracellular IL-10 concentration 3 hr after LPS treatment ($n$ = 4). (f) Representative anti-phospho-NF-κB p65 (Ser536) (top) and anti-total NF-κB p65 (bottom) immunoblot after 24 hr treatment with 0.1 μg/ml LPS with anti-GAPDH loading control. (g) Densitometric analysis of (f): anti-phospho-NF-κB p65 (Ser536) fluorescence as a ratio of anti-total NF-κB p65 normalized to anti-GAPDH fluorescence and represented as fold change in fluorescence from the mean of vehicle-treated controls ($n$ = 8). (h) Extracellular TNF-α concentration 24 hr after LPS treatment ($n$ = 6). (i) Extracellular IL-6 concentration 24 hr after LPS treatment ($n$ = 6). (j) Extracellular IL-10 concentration 24 hr after LPS treatment ($n$ = 5). Unpaired $t$ test, ** $p < .01$, *** $p < .001$, **** $p < .0001$. Data are expressed as mean ± *SEM* [Color figure can be viewed at wileyonlinelibrary.com]

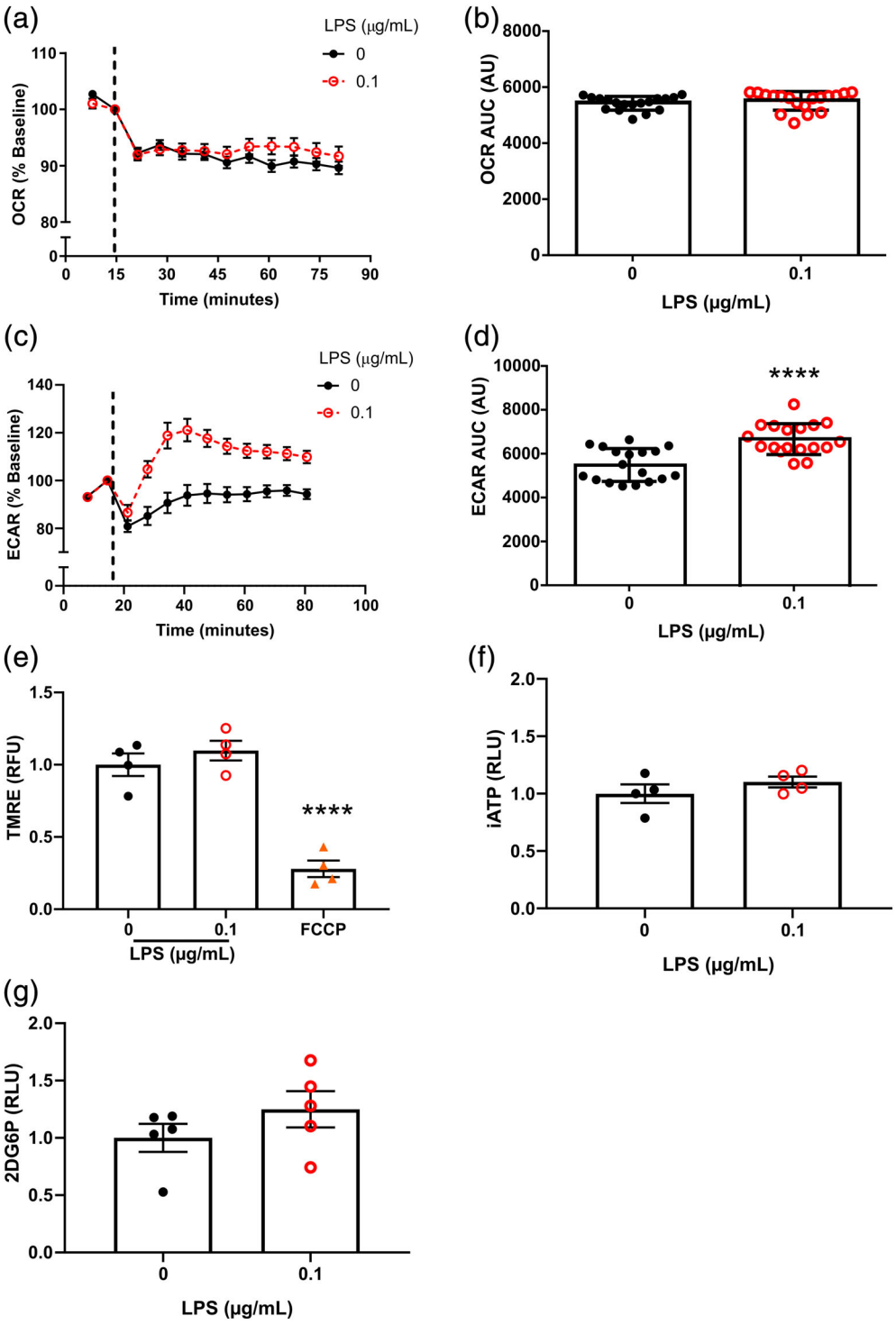


**FIGURE 2** Lipopolysaccharide (LPS) increased glycolytic rate in mouse primary astrocytes within 30 min posttreatment. (a) Oxidative phosphorylation rate, represented as oxygen consumption rate (OCR) over time, of cortical primary mouse astrocytes (CRTAS). Treatment point indicated by vertical dotted line. LPS treatment compared with vehicle-treated control (0.017 mM fatty acid free bovine serum albumin; $n$ = 18, two independent plates). (b) Area under the curve (AUC) of OCR after treatment with LPS (unpaired $t$ test, $p > .05$; $n$ = 18, two independent plates). (c) Glycolysis represented as extracellular acidification rate (ECAR) over time of CRTAS after treatment with LPS ($n$ = 18, two independent plates). (d) AUC of ECAR after treatment with LPS (unpaired $t$ test, **** $p < .0001$; $n$ = 18, two independent plates). (e) Mitochondrial membrane potential represented as fold change from mean of controls, measured by tetramethylrhodamine ethyl ester (TMRE) dye uptake after 15 min treatment with LPS. A total of 10 μM FCCP was used as a positive control (one-way analysis of variance [ANOVA] with post hoc Tukey, **** $p < .0001$; $n$ = 4). (e) Fold change in intracellular ATP (iATP) in CRTAS after 15 min treatment with LPS (unpaired $t$ test, $p > .05$; $n$ = 4). (g) Glucose uptake by mouse primary astrocytes after 15 min treatment with LPS represented as fold change in 2DG6P (unpaired $t$ test, $p > .05$; $n$ = 5). Data are expressed as mean ± *SEM* [Color figure can be viewed at wileyonlinelibrary.com]

## 2.12 | Data presentation and statistics

Data were processed using Microsoft Excel 2013. GraphPad Prism 8 was used to present data and for statistical analyses. For comparisons between two groups, unpaired $t$ tests were used. For multiple comparisons, one-way analysis of variance with post hoc Tukey's tests were used. A minimum of three independent replicates were used for each study. Data are presented as mean ± *SEM*. Statistical significance was taken as $p < .05$.

# 3 | RESULTS

## 3.1 | LPS stimulated NF-κB signaling and cytokine secretion in mouse primary astrocytes

Compared to vehicle-treated control cells, NF-κB (p65) phosphorylation in astrocytes was increased 3 and 24 hr after LPS treatment (113.8%, $p$ = .0031 and 93.9%, $p$ = .0058, respectively; Figure 1a,b

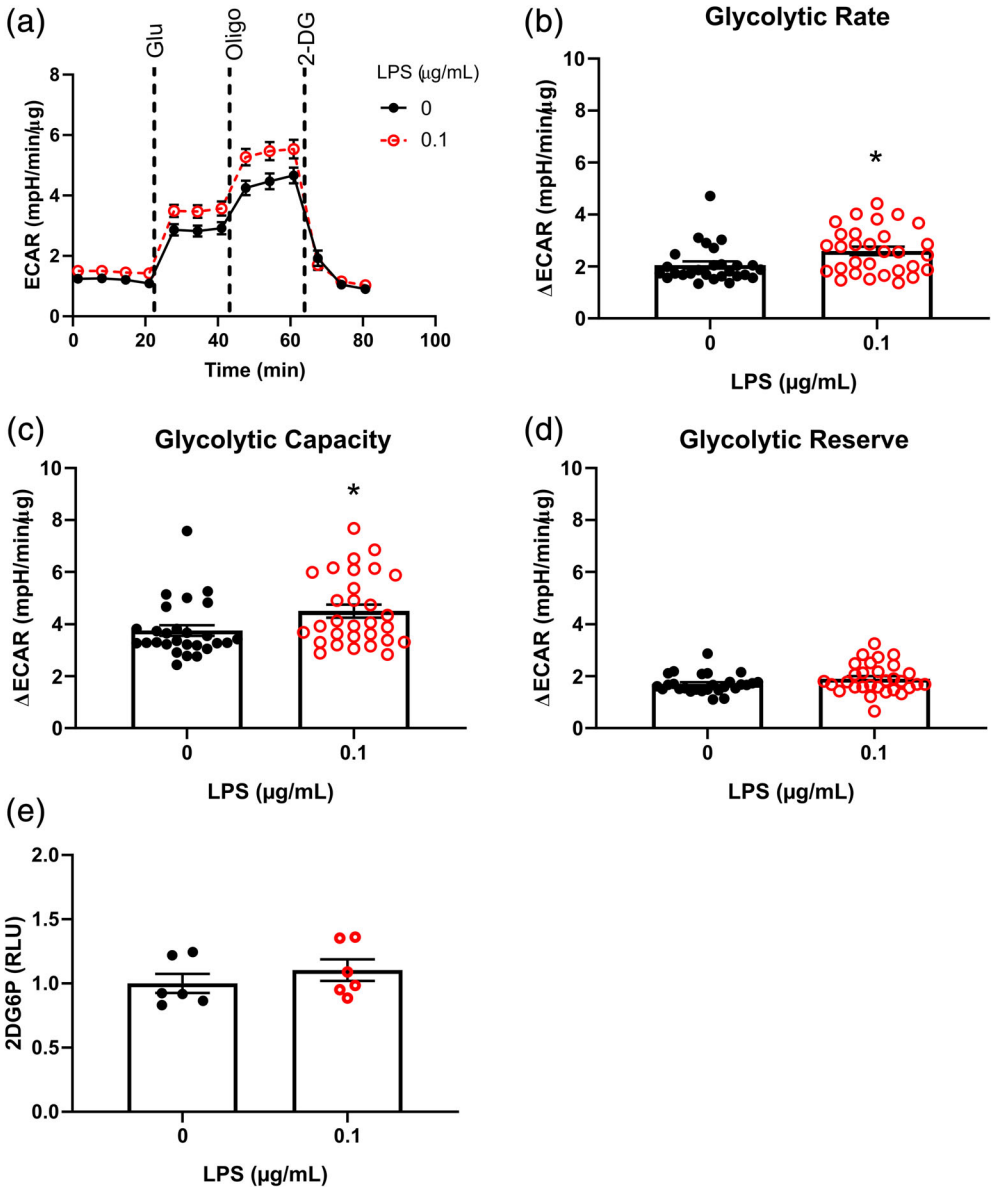


**FIGURE 3** Glycolytic rate and capacity were increased in mouse primary cortical astrocytes after 3 hr treatment with lipopolysaccharide (LPS). (a) Extracellular acidification rate (ECAR) during Glycolytic Stress Test of mouse primary cortical astrocytes 3 hr after treatment with LPS compared with vehicle-treated control (0.017 mM fatty acid free bovine serum albumin; $n = 30$, two independent plates). Glu = 10 mM glucose; Oligo = 1 µM oligomycin; 2-DG = 50 mM 2-deoxyglucose. (b) Glycolytic rate: change in ECAR after treatment with glucose (unpaired $t$ test, * $p < .05$; $n = 30$, two independent plates). (c) Glycolytic capacity: change in ECAR after treatment with oligomycin (unpaired $t$ test, * $p < .05$; $n = 30$, two independent plates). (d) Glycolytic reserve: difference between glycolytic rate and glycolytic capacity (unpaired $t$ test, $p > .05$; $n = 30$, two independent plates). (e) Glucose uptake after 3 hr treatment with LPS as fold change in 2DG6P luminescence (unpaired $t$ test, $p > .05$; $n = 6$). Data are expressed as mean ± *SEM* [Color figure can be viewed at wileyonlinelibrary.com]

and Figure 1f,g; supplementary Figures S7a,b and S8a,b). After 3 hr of treatment with LPS, astrocyte TNF-α release was increased (Figure 1c; $p < .0001$) but neither IL-6 (Figure 1e) nor IL-10 (Figure 1g) release were changed, in comparison to vehicle-treated controls. After 24 hr of LPS treatment, astrocyte release of TNF-α, IL-6, and IL-10 were all increased compared to vehicle-treated controls ($p < .0001$, $p = .0002$, and $p = .0028$, respectively; Figure 1d,f,h). Astrocyte viability was not negatively affected by treatment with LPS after 24 hr, with >90% cell viability, in both LPS and vehicle-treated control groups (supplementary Figure S2b).

## 3.2 | LPS induced an acute increase in glycolytic rate in mouse primary astrocytes

Following measurement of baseline, the astrocytes were treated with LPS or vehicle and OCR (Figure 2a,b) and ECAR (Figure 2c,d) measured every 6 min for 1 hr using the Seahorse Bioanalyzer XF$^{e}$96. No acute change in OCR was observed (Figure 2a,b), indicating that oxidative phosphorylation was not altered. However, there was a rapid 20% increase in ECAR indicating increased glycolytic rate (Figure 2c,d). As a complementary measure of mitochondrial activity, mitochondrial membrane potential was assessed 15 min after treatment with LPS using TMRE dye uptake (Figure 2e). There was no change in mitochondrial membrane potential in LPS-treated astrocytes compared to vehicle-treated controls ($p = .58$), while the positive control, the mitochondrial oxidative phosphorylation uncoupler FCCP, significantly reduced TMRE uptake by 72% ($p < .0001$; Figure 2e). This suggests that the integrity of the mitochondrial membrane was not immediately altered by LPS treatment, and rate of proton flow across the membrane was unaltered. Astrocyte iATP concentrations were also unchanged after 15 min of treatment with LPS in comparison to vehicle-treated controls ($p = .31$; Figure 2f). There was a 25% increase in

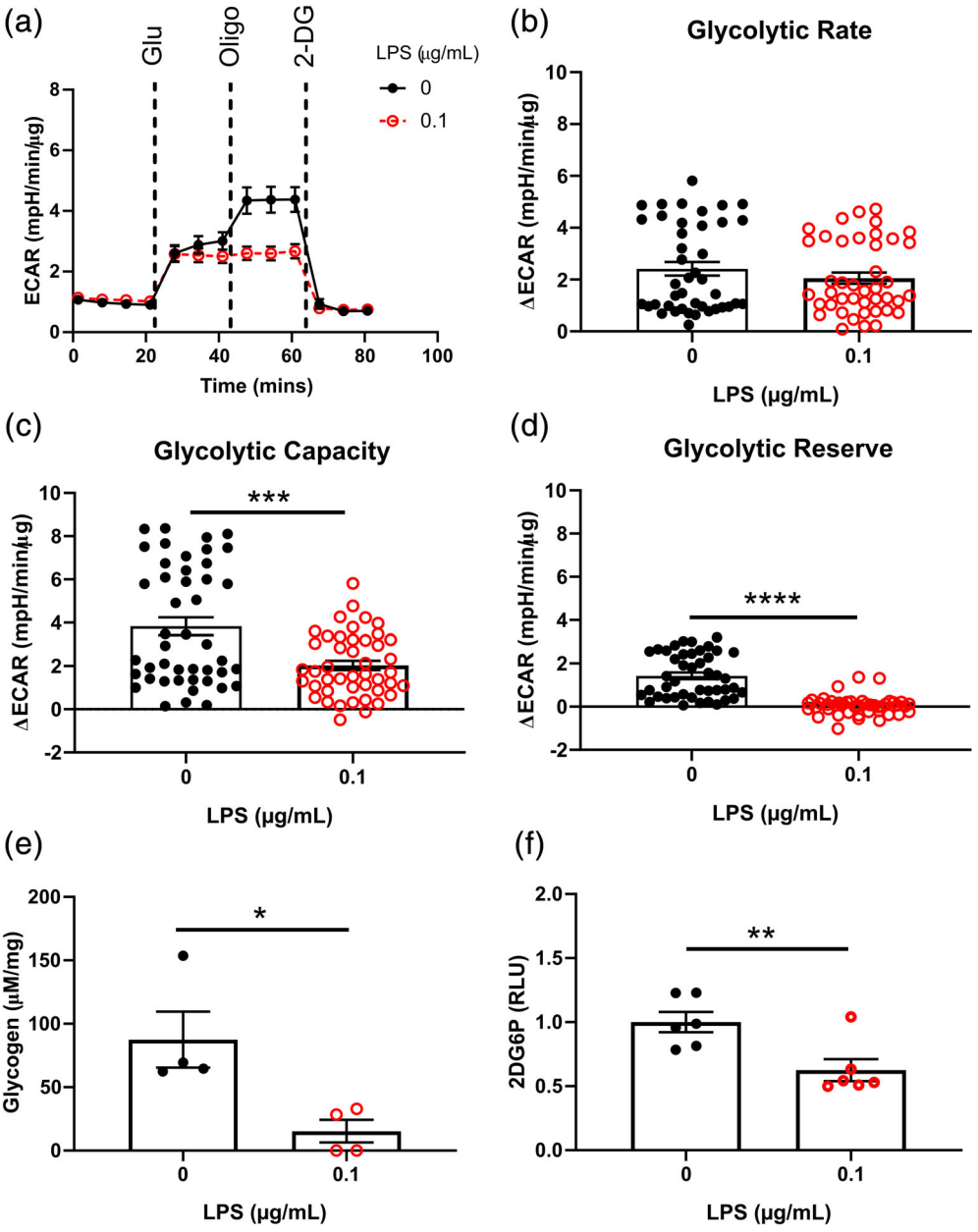


**FIGURE 4** Glycolytic capacity in mouse primary astrocytes was reduced after 24 hr lipopolysaccharide (LPS) treatment. (a) Extracellular acidification rate (ECAR) during Glycolytic Stress Test of mouse primary cortical astrocytes 24 hr after treatment with LPS compared with vehicle-treated control (0.017 mM fatty acid free bovine serum albumin; $n = 44$, three independent plates). Glu = 10 mM glucose; Oligo = 1 µM oligomycin; 2-DG = 50 mM 2-deoxyglucose. (b) Glycolytic rate: change in ECAR after treatment with glucose (unpaired $t$ test, $p > .05$; $n = 44$, three independent plates). (c) Glycolytic capacity: change in ECAR after treatment with oligomycin (unpaired $t$ test, *** $p < .001$; $n = 44$, three independent plates). (d) Glycolytic reserve: difference between glycolytic rate and glycolytic capacity (unpaired $t$ test, **** $p < .0001$; $n = 44$, three independent plates). (e) Intracellular glycogen content after 24 hr treatment with LPS (unpaired $t$ test, * $p < .05$; $n = 4$). (f) Glucose uptake after 24 hr treatment with LPS as fold change in 2DG6P luminescence compared to the mean of vehicle-treated controls (unpaired $t$ test, ** $p < .01$; $n = 6$). Data are expressed as mean ± *SEM* [Color figure can be viewed at wileyonlinelibrary.com]

glucose uptake rate in the cells after 15 min treatment with LPS in comparison to vehicle-treated controls; however, this did not reach statistical significance ($p = .24$; Figure 2g).

### 3.3 | Changes to glycolytic metabolism were maintained 3 hr after treatment with LPS in mouse primary astrocytes

To further interrogate the changes in cellular metabolism related to inflammation, mouse primary astrocytes were treated with LPS for 3 hr and subjected to a Glycolytic Stress Test. Glycolytic rate and capacity were both significantly increased by 26% ($p = .0138$) and 20% ($p = .025$), respectively (Figure 3a–c). This change in extracellular acidification was unlikely to be due to dissolved $CO_2$ from oxidative phosphorylation, as OCR was not increased during the same treatment protocol (supplementary Figure S3). However, while the glucose uptake assay indicated a 10% increase (Figure 3e) in cells treated with LPS for 3 hr compared to vehicle-treated controls, this was not statistically significant ($p = .46$). The glycolytic reserve was unchanged between LPS-treated astrocytes and vehicle-treated controls (Figure 3d).

The Mito Stress Test was used to evaluate mitochondrial function after 3 hr of LPS treatment and no changes were observed compared to vehicle-treated controls (supplementary Figure S3a,d–h). Furthermore, 3 hr of LPS treatment did not impact TMRE uptake compared to vehicle-treated astrocytes (supplementary Figure S3b), in contrast

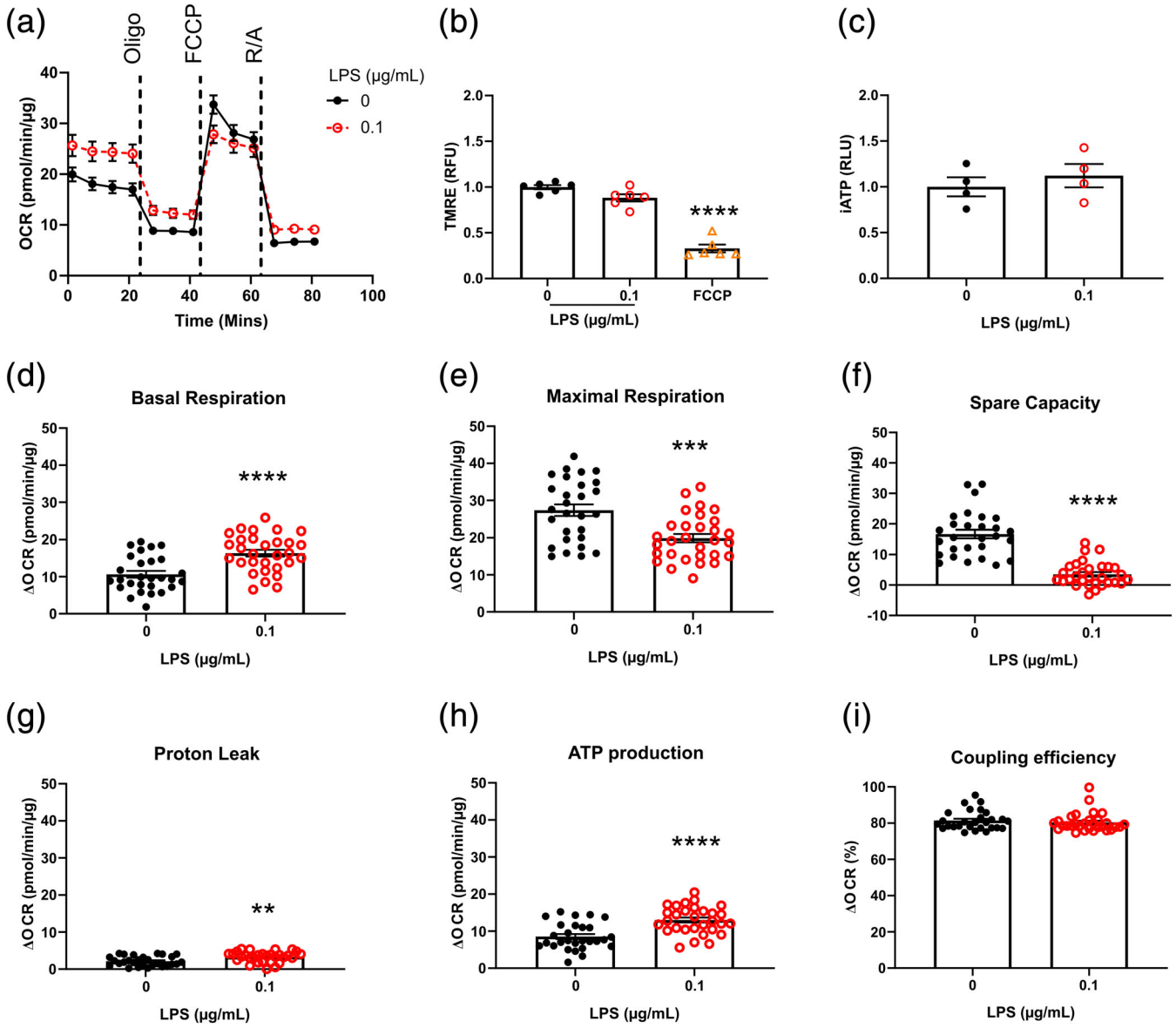


**FIGURE 5** Twenty-four hours exposure to lipopolysaccharide (LPS) increased mitochondrial respiration in mouse primary astrocytes. (a) Oxygen consumption rate (OCR) during Mito Stress Test of mouse primary cortical astrocytes 24 hr after treatment with LPS compared with vehicle-treated control (0.017 mM fatty acid free bovine serum albumin; $n$ = 28–30, 2 independent plates). Oligo = 0.5 µM oligomycin; FCCP = 1 µM; R/A = 0.5 µM rotenone/antimycin. (b) Mitochondrial membrane potential after 24 hr treatment with LPS as fold change from the means of vehicle-treated controls measured by tetramethylrhodamine ethyl ester (TMRE) dye uptake. A total of 10 µM FCCP was used as a positive depolarization control (one-way analysis of variance (ANOVA) with post hoc Tukey, **** $p$ < .0001; $n$ = 6). (c) Intracellular ATP (iATP) after 24 hr treatment with LPS as fold change from the mean of vehicle-treated controls (unpaired $t$ test, $p$ > .05; $n$ = 4). (d) Basal respiration: difference in OCR prior to oligomycin injection and after rotenone/antimycin injection (unpaired $t$ test, **** $p$ < .0001; $n$ = 28–30, two independent plates). (e) Maximal respiration: difference in OCR after injection of FCCP and after rotenone/antimycin injection (unpaired $t$ test, *** $p$ < .001; $n$ = 28–30, two independent plates). (f) Spare capacity: difference in OCR between basal respiration (d) and maximal respiration (e; unpaired $t$ test, **** $p$ < .0001; $n$ = 28–30, two independent plates). (g) Proton leak: difference in OCR after oligomycin injection and after rotenone/antimycin injection (unpaired $t$ test, ** $p$ < .01; $n$ = 28–30, two independent plates). (h) ATP production: difference in OCR prior to oligomycin injection and after oligomycin injection (unpaired $t$ test, **** $p$ < .0001; $n$ = 28–30, two independent plates). (i) Coupling efficiency: percentage of basal respiration (d) used for ATP production (h; unpaired $t$ test, $p$ > .05; $n$ = 28–30, two independent plates). Data are presented as mean ± *SEM* [Color figure can be viewed at wileyonlinelibrary.com]

to the FCCP-treated (positive control) cells which showed a 70% reduction in TMRE uptake ($p$ < .0001). This suggests that astrocyte mitochondrial membrane integrity was unaltered, and coupling was not impacted 3 hr after LPS treatment. iATP concentrations were also unchanged (supplementary Figure S3). Together these data suggest that while there were adaptive changes in glycolysis, mitochondrial metabolism was unchanged by 3 hr of treatment with LPS.

### 3.4 | The glycolytic capacity of mouse primary astrocytes was reduced after 24 hr treatment with LPS

Mouse primary astrocytes were treated with LPS for 24 hr prior to evaluation using the Glycolytic Stress Test. In contrast to the acute (3 hr) treatment, after 24 hr of LPS treatment, there was no significant difference in glycolytic rate between LPS- and vehicle-treated cells (Figure 4a,b; $p = .29$). However, glycolytic capacity was reduced by 47% in the LPS-treated astrocytes in comparison to vehicle-treated controls (Figure 4c; $p = .0002$), resulting in a 97% decrease in glycolytic reserve (Figure 4d; $p < .0001$). This was reflected in a 82% depletion of intracellular glycogen (Figure 4e; $p = .023$). This reduction in glycogen stores and glycolytic capacity may have been due, at least in part, to the 37% reduction in the rate of glucose uptake seen in the 24 hr LPS-treated cells, compared to vehicle-treated controls (Figure 4f; $p = .0091$). These data show that after 24 hr of exposure to LPS, astrocytes undergo pronounced changes in their cellular metabolism, characterized by a reduction in both the glucose uptake and glycolytic capacity.

### 3.5 | Mitochondrial respiration in mouse primary astrocytes was altered after 24 hr of LPS treatment

Given the adaptive changes to glycolysis observed after 24 hr of LPS treatment, the impact on mitochondrial metabolism was also investigated. Treatment with LPS for 24 hr increased basal mitochondrial respiration in astrocytes by 53% in comparison to vehicle-treated controls (Figure 5a,d; $p < .0001$). Conversely, maximal mitochondrial respiration was reduced by 27% (Figure 5e; $p = .0003$), resulting in a 79% reduction in spare capacity (Figure 5f; $p < .0001$). Proton leak was increased by 54% (Figure 5g; $p = .0019$). Mitochondrial ATP production was increased by 52% (Figure 5h; $p < .0001$) and total iATP levels were unchanged after 24 hr treatment with LPS compared to vehicle-treated cells (Figure 5c; $p = .48$). The mitochondrial coupling efficiency was unchanged (Figure 5i) and there was no difference in TMRE dye uptake between cells treated with LPS for 24 hr and vehicle-treated controls (Figure 5b). This corroborates the observed absence of change in coupling efficiency. Together these data suggest after 24 hr of LPS treatment basal mitochondrial activity of mouse primary astrocytes is increased, despite reduced mitochondrial capacity. Combined with the results of the Glycolytic Stress Test, these data suggest that astrocytes alter their metabolism to maintain iATP through altered substrate preference.

### 3.6 | Glucose transporter 1 expression was reduced by 24 hr of LPS treatment in mouse primary astrocytes

To investigate potential causes of the reduced glycolytic capacity observed after 24 hr LPS treatment, glucose transporter 1 (GLUT1) glucose transporter expression was quantified using immunoblotting. After 3 hr of LPS treatment GLUT1 expression was not altered compared to vehicle-treated controls (Figure 6a; supplementary Figure S9a; $p = .96$). In line with the observed alterations in glycolytic rate and capacity (Figure 4a–d) and in concordance with the glucose uptake data (Figure 4f), 24 hr of treatment with LPS significantly reduced GLUT1 expression in astrocytes compared to vehicle-treated controls (Figure 6b; supplementary Figure S8b; $p = .0044$).

### 3.7 | NF-κB inhibition reduced baseline glycolytic metabolism and prevented LPS induced increases in glycolytic rate

In other cell types, NF-κB signaling is implicated in the regulation of cellular metabolism (Goetzman & Prochownik, 2018;

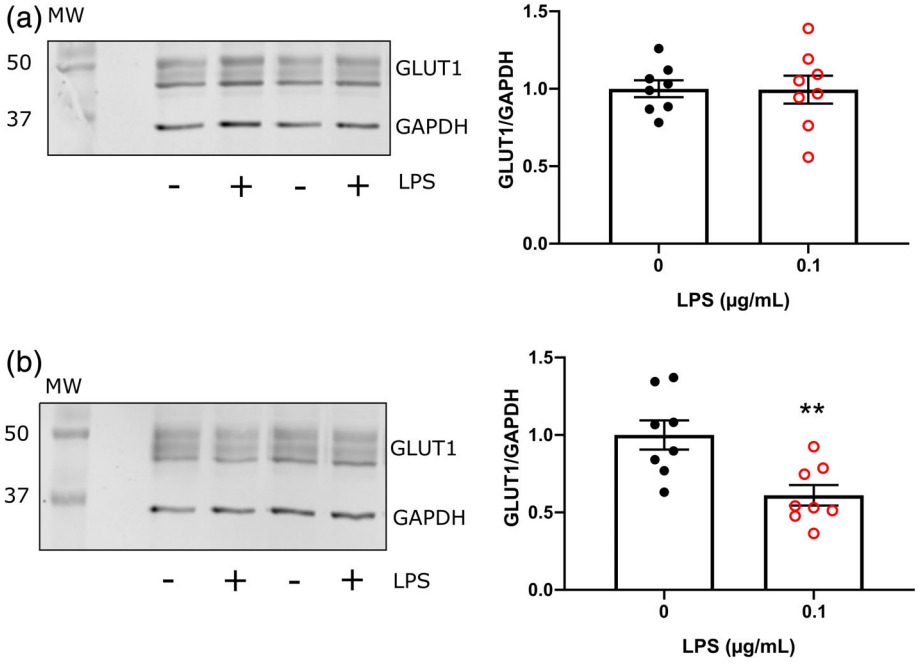


**FIGURE 6** Glucose transporter glucose transporter 1 (GLUT1) expression in mouse primary astrocytes was reduced after 24 hr treatment with lipopolysaccharide (LPS). GLUT1 expression quantified by immunoblotting with anti-GLUT1 (Millipore) after 3 hr treatment (a; $n = 8$) or 24 hr treatment (b; $n = 8$) with 0.1 μg/ml LPS. Left: Representative blot. Right: Densitometric analysis normalized to GAPDH (Protein Tech) and as fold change compared to mean of vehicle-treated controls. Unpaired *t* test, ** $p < .01$ [Color figure can be viewed at wileyonlinelibrary.com]

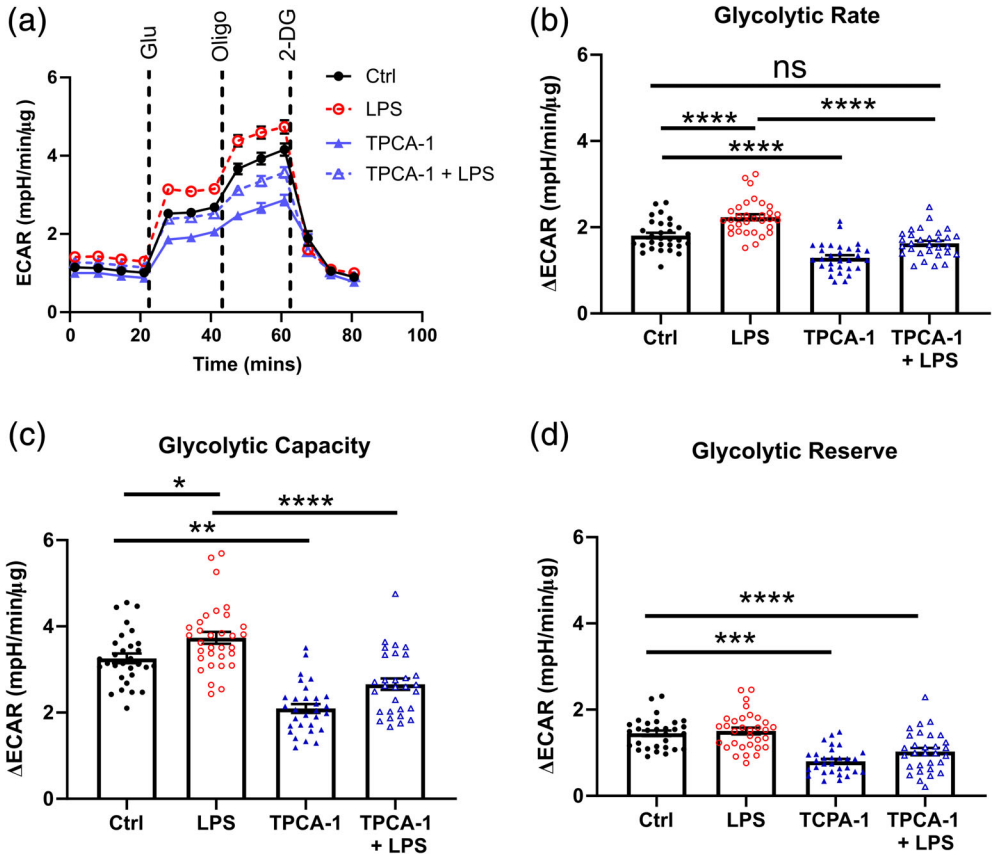


**FIGURE 7** – Inhibition of nuclear factor-kappa B (NF-κB) signaling attenuated the glycolytic response to lipopolysaccharide (LPS) after 3 hr. (a) Extracellular acidification rate (ECAR) during a Glycolytic Stress Test of mouse primary cortical astrocytes after 2 hr pretreatment with NF-κB inhibitor, TPCA-1 (1 μM) ± 3 hr LPS treatment (0.1 μg/ml) compared with vehicle-treated control (Ctrl; 0.017 mM fatty acid free bovine serum albumin/0.01% vol/vol DMSO; $n = 32$, two independent plates). Glu = 10 mM glucose; Oligo = 1 μM oligomycin; 2-DG = 50 mM 2-deoxyglucose. (b) Glycolytic rate: change in ECAR after treatment with glucose (one-way analysis of variance [ANOVA] with post hoc Tukey, **** $p > .0001$, ns $p > .05$; $n = 32$, two independent plates). (c) Glycolytic capacity: change in ECAR after treatment with oligomycin (one-way ANOVA with post hoc Tukey, * $p < .05$, ** $p < .01$, **** $p > .0001$; $n = 32$, two independent plates). (d) Glycolytic reserve: difference between glycolytic rate and glycolytic capacity (one-way ANOVA with post hoc Tukey, *** $p < .001$, **** $p < .0001$; $n = 32$, two independent plates). Data are expressed as mean ± *SEM* [Color figure can be viewed at wileyonlinelibrary.com]

Sommermann, O'Neill, Plas, & Cahir-McFarland, 2011). To investigate this in astrocytes, the IKK-β inhibitor TPCA-1, was used. TPCA-1 inhibited the inflammatory response to LPS after 3 and 24 hr of treatment: TNF-α and IL-6 release were significantly reduced by TPCA-1 (supplementary Figure S4a–d; $p < .0001$), which also prevented the LPS-induced increase in NF-κB p65 (Ser536) phosphorylation relative to total NF-κB (p65) expression at 24 hr (supplementary Figure S4e,f, supplementary Figures S7c and S8c; $p < .0001$). TPCA-1 treatment had no impact on cell viability (supplementary Figure S2d; $p = .95$).

Astrocytes receiving the combined TPCA-1 and LPS (3 hr) treatment displayed a 27% reduction in glycolytic rate compared to those treated with LPS alone (Figure 7a,b; $p < .0001$) suggesting that NF-κB signaling plays an instrumental role in the glycolytic response to LPS. Importantly, treatment with TPCA-1 alone reduced glycolytic rate by 28% compared to vehicle-treated cells (Figure 7a,b; $p < .0001$). This suggests that NF-κB signaling plays an important role in regulating basal metabolism in astrocytes which may impact the extent of the LPS-induced response. Glycolytic capacity was also significantly reduced in TPCA-1 cells in the presence (29%; $p < .0001$) or absence of LPS (36%; $p < .0001$) compared to controls (Figure 7c,d). This resulted in a reduction of glycolytic reserve in TPCA-1 groups (32% with LPS and 45% without LPS treatment; both $p < .0001$).

Compared to vehicle-treated controls, TPCA-1 treatment did not change mitochondrial maximal respiration, proton leak, spare capacity, or iATP in the presence or absence of LPS (supplementary Figure S5c, d,f,h, respectively). However, TPCA-1 treatment with LPS significantly increased basal respiration by 18% (supplementary Figure S5a,b; $p = .01$), increasing mitochondrial ATP production by 21% (supplementary Figure S5e; $p = .002$).

### 3.8 | Metabolic consequences of prolonged exposure to LPS were abolished through inhibition of NF-κB signaling

TPCA-1 treatment did not alter astrocyte glycolytic rate after 24 hr in the presence or absence of LPS (Figure 8a,b). Treatment with TPCA-1

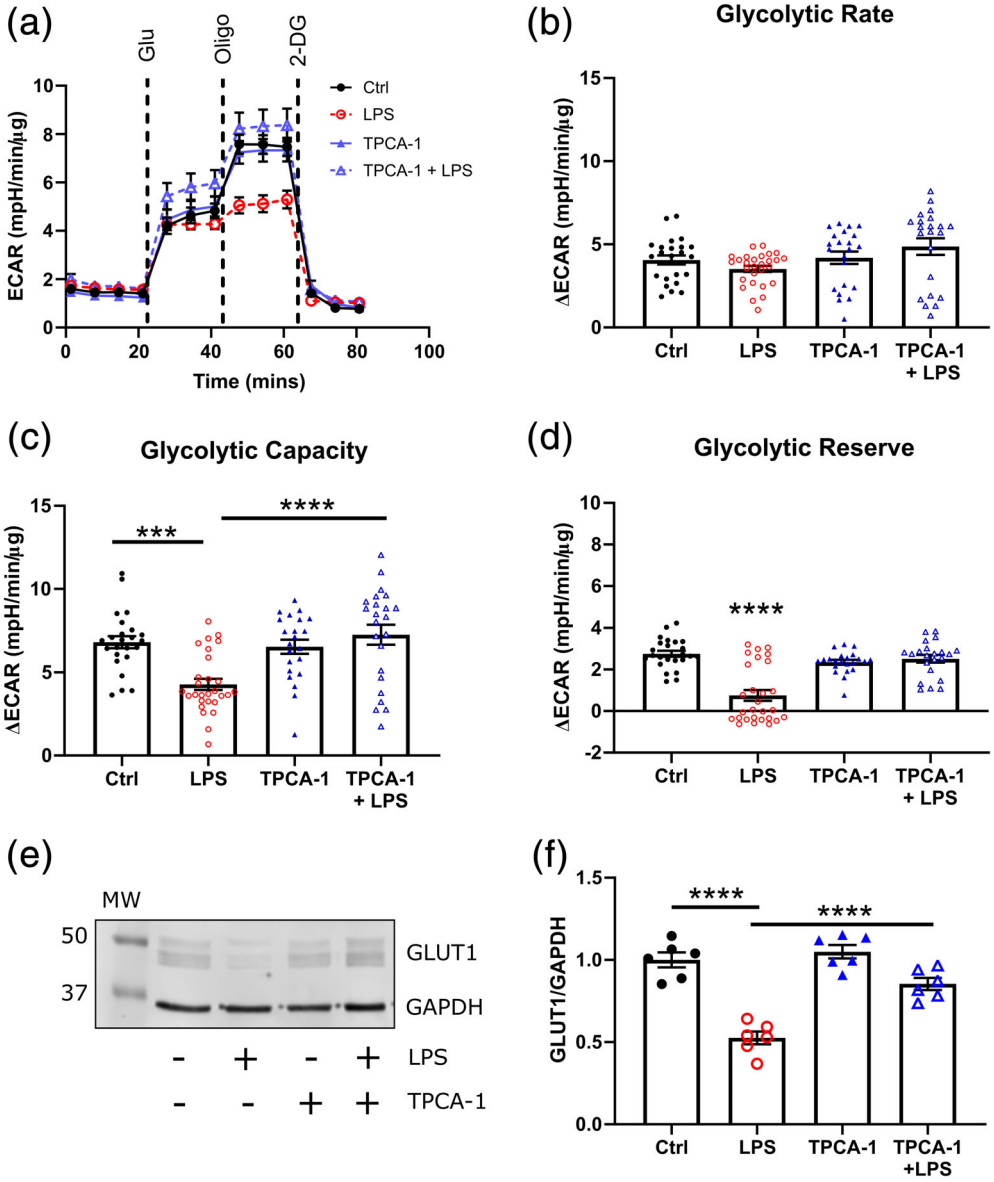


**FIGURE 8** Inhibition of nuclear factor-kappa B (NF-κB) rescued the lipopolysaccharide (LPS) induced reduction in glycolytic capacity 24 hr after treatment. (a) Extracellular acidification rate (ECAR) during a Glycolytic Stress Test of mouse primary cortical astrocytes after 2 hr pretreatment with NF-κB inhibitor, TPCA-1 (1 μM) ± 24 hr LPS treatment (0.1 μg/ml) compared with vehicle-treated control (Ctrl; 0.017 mM fatty acid free bovine serum albumin/0.01% vol/vol DMSO; $n$ = 22–28, two independent plates). Glu = 10 mM glucose; Oligo = 1 μM oligomycin; 2-DG = 50 mM 2-deoxyglucose. (b) Glycolytic rate: change in ECAR after treatment with 10 mM glucose (one-way analysis of variance [ANOVA] with post hoc Tukey, $p > .05$; $n$ = 22–28, two independent plates). (c) Glycolytic capacity: change in ECAR after treatment with oligomycin (one-way ANOVA with post hoc Tukey, *** $p < .001$, **** $p < .0001$; $n$ = 22–28, two independent plates). (d) Glycolytic reserve: difference between glycolytic rate and glycolytic capacity (one-way ANOVA with post hoc Tukey, **** $p < .0001$; $n$ = 22–28, two independent plates). (e) Representative blot immunoblot of glucose transporter 1 (GLUT1) expression with GAPDH loading control after 2 hr pretreatment with NF-κB inhibitor TPCA-1 (1 μM) and 24 hr treatment with 0.1 μg/ml LPS. (f) Densitometric analysis of (e) (one-way ANOVA with post hoc Tukey, **** $p < .0001$, $n$ = 6). Data are expressed as mean ± *SEM* [Color figure can be viewed at wileyonlinelibrary.com]

prevented the 24 hr LPS-induced decrease in glycolytic capacity (37%; $p = .0003$; Figure 8c) and reserve (72%; $p < .0001$; Figure 8d), but TPCA-1 alone did not alter glycolytic capacity or reserve when compared to vehicle-treated astrocytes. Additionally, the LPS-induced reduction in GLUT-1 expression after 24 hr (–47%; $p < .0001$) was attenuated by TPCA-1 pretreatment (Figure 8e,f; supplementary Figure S9c; $p = .081$).

In astrocytes TPCA-1 treatment reduced the 24 hr LPS-induced increases in basal respiration (65%; $p < .0001$), proton leak (84%; $p < .0001$), and mitochondrial ATP production (61%; $p < .0001$) (Figure 9a,b,d,e). Maximal respiration was reduced by TPCA-1 in the presence of LPS treatment (35%; $p < .0001$), which was greater than the reduction induced by LPS alone (18%; $p = .013$). Treatment with

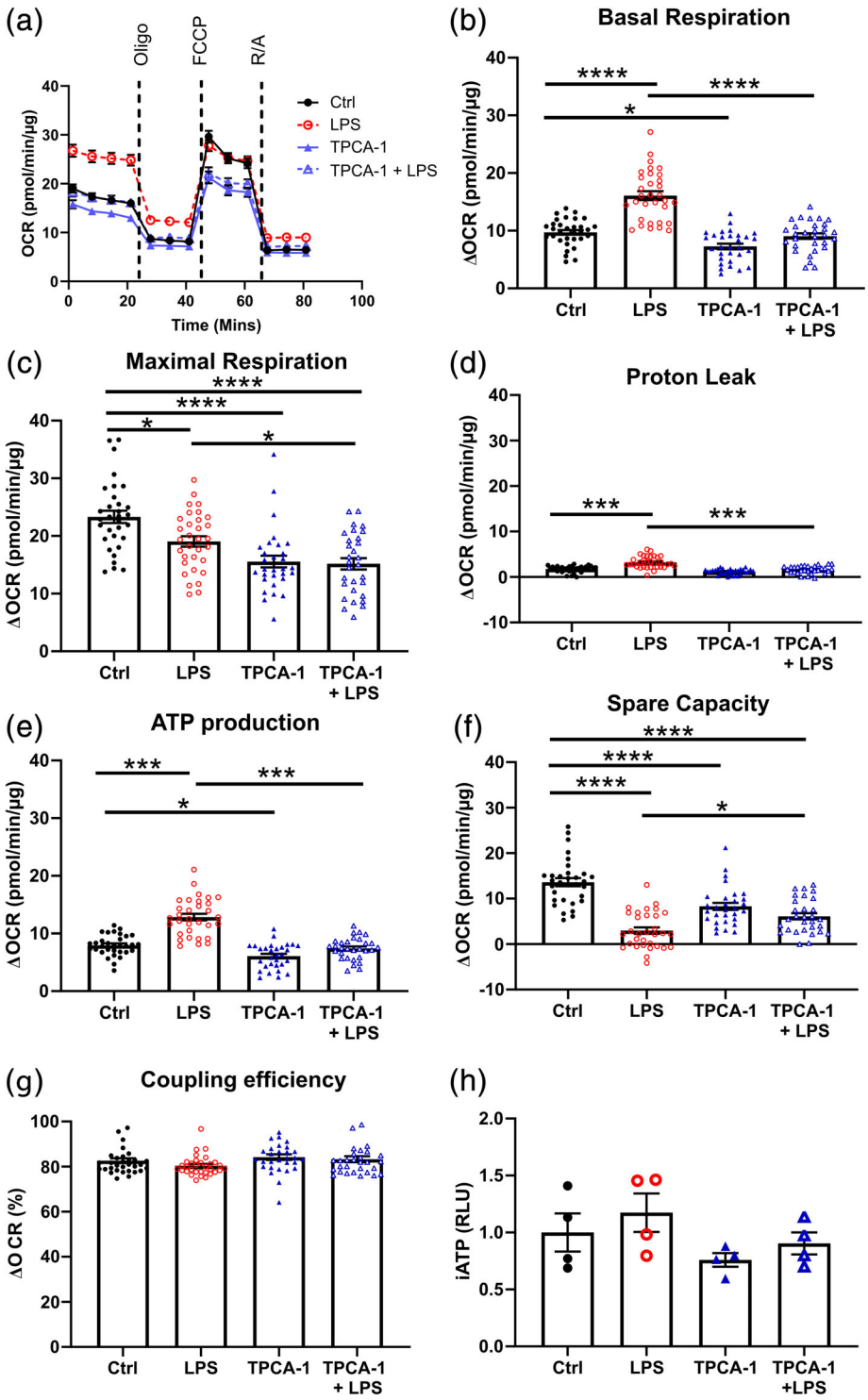


**FIGURE 9** Inhibition of nuclear factor-kappa B (NF-κB) altered mitochondrial respiration independently from lipopolysaccharide (LPS) treatment after 24 hr. (a) Oxygen consumption rate (OCR) during a Mito Stress Test of mouse primary cortical astrocytes after 2 hr pretreatment with NF-κB inhibitor, TPCA-1 (1 μM) ± 24 hr LPS treatment (0.1 μg/ml) compared with vehicle-treated control (Ctrl; 0.017 mM fatty acid free bovine serum albumin/0.01% vol/vol DMSO; $n = 30$, two independent plates). Oligo = 0.5 μM oligomycin; FCCP = 1 μM; R/A = 0.5 μM rotenone/antimycin. (b) Basal respiration: difference in OCR prior to oligomycin injection and after rotenone/antimycin injection (one-way analysis of variance [ANOVA] with post hoc Tukey, **** $p < .0001$, * $p < .05$; $n = 30$, two independent plates). (c) Maximal respiration: difference in OCR after injection of FCCP and after rotenone/antimycin injection (one-way ANOVA with post hoc Tukey, **** $p < .0001$, * $p < .05$; $n = 30$, two independent plates). (d) Proton leak: difference in OCR after oligomycin injection and after rotenone/antimycin injection (one-way ANOVA with post hoc Tukey, *** $p < .001$; $n = 30$, two independent plates). (e) ATP production: difference in OCR prior to oligomycin injection and after oligomycin injection (one-way ANOVA with post hoc Tukey, *** $p < .001$, * $p < .05$; $n = 30$, two independent plates). (f) Spare capacity: difference in OCR between basal respiration (b) and maximal respiration (c; one-way ANOVA with post hoc Tukey, **** $p < .0001$, * $p < .05$; $n = 30$, two independent plates). (g) Coupling efficiency: percentage of basal respiration (b) used for ATP production (d; one-way ANOVA with post hoc Tukey, $p > .05$; $n = 30$, two independent plates). (h) Intracellular ATP (iATP) represented as fold change in luminescence from the mean of vehicle-treated controls (one-way ANOVA with post hoc Tukey, $p > .05$; $n = 4$). Data are presented as mean ± *SEM* [Color figure can be viewed at wileyonlinelibrary.com]

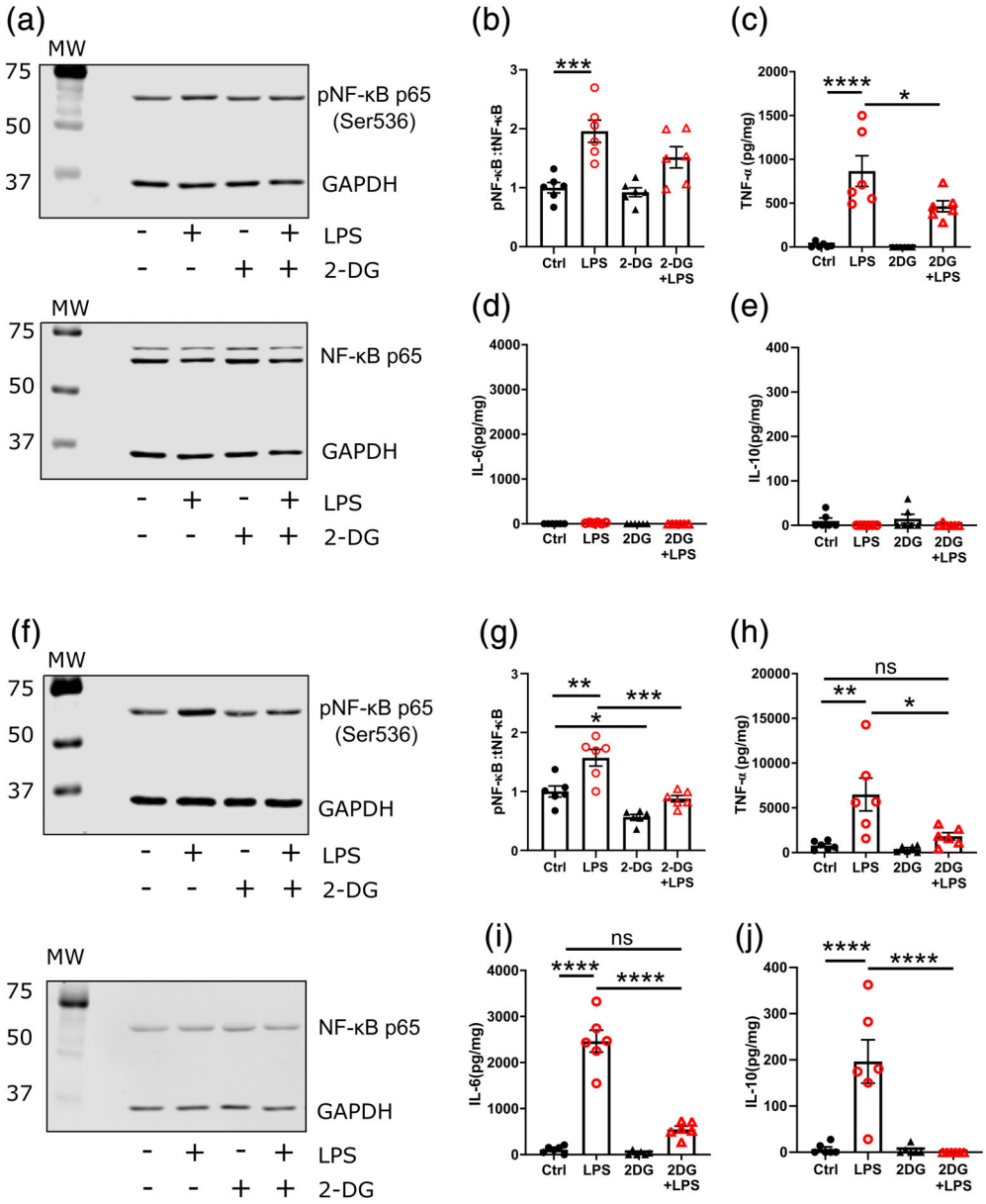


**FIGURE 10** Inhibition of glycolysis reduced lipopolysaccharide (LPS) stimulated cytokine release. (a) Representative anti-phospho-nuclear factor-kappa B (NF-κB) p65 (Ser536) (top) and anti-total NF-κB p65 (bottom) immunoblot after 2 hr pretreatment with 10 mM 2-deoxyglucose (2-DG) ± 3 hr treatment with 0.1 μg/ml LPS with anti-GAPDH loading control. (b) Densitometric analysis of (a): anti-phospho-NF-κB p65 (Ser536) fluorescence as a ratio of anti-total NF-κB p65 normalized to anti-GAPDH fluorescence and represented as fold change in fluorescence from the mean of vehicle-treated controls ($n$ = 6). (c) Extracellular TNF-α concentration after 2 hr pretreatment with 10 mM 2-DG ± 3 hr LPS treatment ($n$ = 6). (d) Extracellular IL-6 concentration after 2 hr pretreatment with 10 mM 2-DG ± 3 hr LPS treatment ($n$ = 6). (e) Extracellular IL-10 concentration after 2 hr pretreatment with 10 mM 2-DG ± 3 hr LPS treatment ($n$ = 6). (f) Representative anti-phospho-NF-κB p65 (Ser536) (top) and anti-total NF-κB p65 (bottom) immunoblot after 2 hr pretreatment with 10 mM 2-DG and 24 hr treatment with 0.1 μg/ml LPS with anti-GAPDH loading control. For this experiment, the antibody used was sourced from NEB #8242, and used to probe a separate immunoblot from that probed with anti-phospho-NF-κB antibody. (g) Densitometric analysis of (f): anti-phospho-NF-κB p65 (Ser536) fluorescence as a ratio of anti-total NF-κB p65 normalized to anti-GAPDH fluorescence and represented as fold change in fluorescence from the mean of vehicle-treated controls ($n$ = 6). (h) Extracellular TNF-α concentration after 2 hr pretreatment with 10 mM 2-DG ± 24 hr LPS treatment ($n$ = 6). (i) Extracellular IL-6 concentration after 2 hr pretreatment with 10 mM 2-DG ± 24 hr LPS treatment ($n$ = 6). (j) Extracellular IL-10 concentration after 2 hr pretreatment with 10 mM 2-DG ± 24 hr LPS treatment ($n$ = 6). One-way analysis of variance (ANOVA) with post hoc Tukey, ns $p > .05$, * $p < .05$, ** $p < .01$, **** $p < .0001$. Ctrl—vehicle control. Data are expressed as mean ± *SEM* [Color figure can be viewed at wileyonlinelibrary.com]

TPCA-1 alone reduced basal respiration and ATP production by 25% ($p$ = .013) and 24% ($p$ = .011), respectively (Figure 9a,f). TPCA-1 reduced maximal respiration by 33% ($p$ < .0001), independently of LPS treatment, suggesting that NF-κB signaling may play a role in normal mitochondrial metabolism, which was attenuated by TPCA-1. TPCA-1 treatment attenuated the LPS-induced reduction in spare

capacity by 23% (Figure 9f; $p < .0001$). No significant change was seen in coupling efficiency after treatment with TPCA-1 (Figure 9g). iATP levels were not altered (Figure 9h).

### 3.9 | Inhibition of the metabolic response to LPS attenuated cytokine release from mouse primary astrocytes

To investigate the necessity of glycolytic metabolism for the astrocyte inflammatory response, cells were pretreated with the non-metabolizable glucose analogue, 2-DG (10 mM) prior to stimulation with LPS. Confirming the inhibitory effect of 2-DG on glycolysis, mouse primary astrocytes treated with 2-DG showed a 36% reduction in ECAR ($p < .0001$) but no impact was observed on OCR (supplementary Figure S6). Then, 24 hr treatment with 2-DG caused a 2% decrease in cell viability which, while statistically significant ($p < .0001$; supplementary Figure S2c), was unlikely to explain the observed changes in metabolism (supplementary Figure S6) and cytokine release (Figure 10c–h). 2-DG pretreatment attenuated the LPS-induced increase in NF-κB (p65) phosphorylation relative to total NF-κB expression in astrocytes 3 hr after LPS treatment (Figure 10a,b; supplementary Figures S7d and S8d; $p = .007$) and abolished the response after 24 hr (Figure 10f,g; supplementary Figures S7e and S8e; $p = .0015$). 2-DG treatment significantly reduced LPS-induced release of TNF-α (Figure 10c,h; 3 hr $p = .03$, 24 hr $p = .0118$) and IL-6 (Figure 10d,i, $p < .0001$) from astrocytes at both 3 and 24 hr and completely abolished IL-10 release at both time points (Figure 10e,j; $p < .0001$).

## 4 | DISCUSSION

In common with the extensive published studies from peripheral immune cells (Bantug, Galluzzi, Kroemer, & Hess, 2018; O'Neill et al., 2016; Russell et al., 2019), our data indicate that astrocytes also display immunometabolic responses. Increases in glucose uptake and glycolytic metabolism were evident in astrocytes within minutes of LPS treatment and by 3 hr post-LPS, the Glycolytic Stress Test revealed an increased rate of glycolysis and glycolytic capacity. Due to the speed of the response, these changes are likely driven by increased activity of glucose transporters and the rate limiting glycolytic enzymes. Inhibition of NF-κB signaling with TPCA-1 abolished the LPS-induced glycolytic response in astrocytes at 3 hr suggesting a key role for this pathway in the observed response. Translocation of GLUT transporters into the plasma membrane is regulated by NF-κB signaling in other cell types (Sommermann et al., 2011). Although no change in total GLUT1 expression was seen at 3 hr after LPS treatment our studies, the subcellular localization of GLUT1 was not assessed; therefore, increased localization of GLUT1 at the plasma membrane cannot be ruled out. NF-κB signaling mediates increases in expression of c-Myc, a transcriptional regulator of glycolytic genes (Goetzman & Prochownik, 2018; La Rosa, Pierce, & Sonenshein, 1994), in fibroblasts and of hexokinase II in sarcoma cells (Londhe et al., 2018). Our results suggest that this pathway may also contribute to the changes seen in astrocytes.

Chronic LPS exposure (24 hr) resulted in metabolic adaptations in astrocytes, probably to maintain ATP production in the face of prolonged insult: Glycolytic capacity and reserve were reduced, but were accompanied by increased mitochondrial metabolism. As the experimental medium used for the Mito Stress Test was supplemented with pyruvate, the increases in mitochondrial metabolism were unlikely to be directly caused by the change in glycolysis reported at this time point. The increase in mitochondrial metabolism was likely driven by increased TCA cycling to enable utilization of alternate fuel sources as it has previously been shown that astrocytes increase TCA cycle rate after 48 hr treatment with IL-1β or TNF-α (Gavillet et al., 2008). We did not measure consumption of alternative carbon sources in this study so we cannot reliably ascertain how the TCA cycle is being supplied in the absence of glucose or glycogen derived carbon in our model. Amino acid availability has been demonstrated to be important for immune responses in macrophages (Viola, Munari, Sánchez-Rodríguez, Scolaro, & Castegna, 2019). Indeed, data from other groups suggests that astrocytes increase metabolism of glutamate during hypoglycemia (Hertz & Hertz, 2003; Nissen, Pajęcka, Stridh, Skytt, & Waagepetersen, 2015). In our model, the astrocytes were supplemented with glutamine; this may enable them to use amino acids to maintain oxidative metabolism during inflammation or absence of glucose, and this could be an interesting avenue for further studies.

In our study, TPCA-1 reduced the LPS-induced increase in mitochondrial activity, suggesting a regulatory role for NF-κB in astrocyte mitochondrial metabolism. In other cell types, NF-κB promotes mitochondrial respiration through increased expression and stabilization of p53 (Aleyasin et al., 2004; Fujioka et al., 2004; Mauro et al., 2011), which may also be the case in astrocytes. p53 activity reduces transcription of GLUT1 (Johnson & Perkins, 2012; Mauro et al., 2011; Schwartzenberg-Bar-Yoseph, Armoni, & Karnieli, 2004), which in our study was significantly reduced by chronic LPS treatment in a NF-κB-dependent manner. This reduced GLUT1 expression may explain the attenuated glycolytic capacity and glucose uptake we observed in astrocytes exposed to LPS for 24 hr. We also reported a depletion of intracellular glycogen stores after 24 hr of LPS treatment. This data are consistent with data from other groups in astrocytes treated with pro-inflammatory cytokines for 48 hr (Bélanger et al., 2011; Gavillet et al., 2008). It is possible that restricting glucose uptake, through downregulating GLUT1 expression, results in depletion of glycogen stores and may be a mechanism by which astrocytes attempt to reduce glycolytic activity to limit the inflammatory response. This conclusion is further supported by the increased concentrations of the anti-inflammatory cytokine IL-10 measured at 24 hr, demonstrating that astrocytes are attempting to mitigate the pro-inflammatory environment by this timepoint.

A reduction in autocrine/paracrine actions of LPS-induced astrocyte cytokine production on metabolism is likely partially responsible for the metabolic differences seen downstream of TPCA-1 inhibition. However, our data indicating reduced mitochondrial metabolism in

astrocytes treated with TPCA-1 for 24 hr also suggests an important regulatory role for NF-κB signaling in basal astrocyte metabolism, probably driven through the mechanism(s) discussed above. This is supported by the observation that treatment with TPCA-1 alone reduced glycolytic rate after 3 hr, suggesting NF-κB plays a role in maintaining basal glycolytic flux in astrocytes. This decrease in glycolytic rate was only evident after addition of glucose, suggesting that after inhibition of NF-κB signaling astrocytes likely have reduced ability to take up exogenous glucose rather than impaired utilization of internal glycogen stores. In addition to inhibiting NF-κB signaling, TPCA-1 has also been reported to inhibit STAT3 signaling (Nan et al., 2014), which can also regulate metabolic function during inflammation (Poli & Camporeale, 2015). As such, a role for STAT3 signaling in mediating the effects seen cannot be ruled out.

Blocking glycolytic function in astrocytes with 2-DG reduced cytokine release and NF-κB (p65) phosphorylation after 24 hr LPS treatment, suggesting reduced activity of the canonical NF-κB pathway. However, NF-κB phosphorylation was still evident 3 hr after LPS treatment despite glycolytic inhibition, perhaps suggesting a role for autocrine/paracrine actions of residual cytokine production in perpetuating the inflammatory response. The initial production of cytokines may be reduced due to 2-DG associated suppression of other inflammatory pathways. For example, the glycolytic enzyme pyruvate kinase isoenzyme M2 acts as a kinase for STAT3 (Gao, Wang, Yang, Liu, & Liu, 2012). Reduced glycolytic flux may lead to lower expression of this enzyme, reducing STAT3 signaling. This would lead to a reduced inflammatory response. Alternatively, the reduced glycolytic rate may prevent the production of carbon intermediates required for cytokine production, through limiting the repurposing of TCA cycle enzymes (Menk et al., 2018; Williams, O'Neill, & O'Neill, 2018). This would result in a negative feedback loop reducing the inflammatory response (Caslin et al., 2018; McGettrick & O'Neill, 2013). It has been reported that in macrophages 2-DG reduces mitochondrial function independently of glycolytic function (Wang et al., 2018); however, in our data there was no change in oxidative rate as a result of 2-DG treatment. This suggests that attenuation of the LPS-induced inflammatory response in the presence of 2-DG was likely a result of glycolytic inhibition rather than modulation of mitochondrial metabolism, but further investigation would be required to confirm this.

In conclusion, we have shown that astrocytes have a rapid and flexible metabolic response to LPS-induced inflammatory insult. This metabolic response was abolished through inhibition of canonical NF-κB signaling using the pharmacological inhibitor TPCA-1, implicating this pathway as a major regulator of inflammatory metabolism in astrocytes. Furthermore, pharmacological inhibition of NF-κB signaling was sufficient to impact metabolism in astrocytes, independent of inflammation, suggesting an integral role for NF-κB in basal astrocyte metabolism. In support of our hypothesis, inhibition of glycolysis attenuated cytokine release from astrocytes, and resulted in inhibition of LPS-induced NF-kB phosphorylation, suggesting that glycolysis in astrocytes is essential for maintaining an inflammatory response. Together these data indicate that in astrocytes metabolic adaptations are necessary for the full inflammatory response to LPS and, in turn, inhibiting NF-κB signaling is sufficient to impact basal metabolism.

## ACKNOWLEDGMENTS

This work was supported by grants from the Medical Research Council (MR/N012763/1 K. L. J. E. and C. B., which supported NMH), Diabetes UK (RD Lawrence Fellowship to C. B.; 13/0004647) and the European Foundation for the Study of Diabetes (to C. B. and KLJE, which supports PGWP), and internal funding from the University of Exeter Medical School (which supports J. L. R.).

## CONFLICT OF INTEREST

The authors declare no potential conflict of interest.

## DATA AVAILABILITY STATEMENT

The datasets used and/or analyzed during the current study are available from the corresponding author on reasonable request.

## ORCID

*Craig Beall* https://orcid.org/0000-0002-4263-0866
*Kate L. J. Ellacott* https://orcid.org/0000-0001-5261-7465

## REFERENCES

Aleyasin, H., Cregan, S. P., Iyirhiaro, G., O'Hare, M. J., Callaghan, S. M., Slack, R. S., & Park, D. S. (2004). Nuclear factor-κB modulates the p53 response in neurons exposed to DNA damage. *The Journal of Neuroscience*, *24*(12), 2963–2973. https://doi.org/10.1523/jneurosci.0155-04.2004

Almeida, A., Moncada, S., & Bolaños, J. P. (2004). Nitric oxide switches on glycolysis through the AMP protein kinase and 6-phosphofructo-2-kinase pathway. *Nature Cell Biology*, *6*(1), 45–51. https://doi.org/10.1038/ncb1080

Bantug, G., Galluzzi, L., Kroemer, G., & Hess, C. (2018). The spectrum of T cell metabolism in health and disease. *Nature Reviews Immunology*, *18*, 19–34. https://doi.org/10.1038/nri.2017.99

Bélanger, M., Allaman, I., & Magistretti, P. J. (2011). Differential effects of pro- and anti-inflammatory cytokines alone or in combinations on the metabolic profile of astrocytes. *Journal of Neurochemistry*, *116*(4), 564–576. https://doi.org/10.1111/j.1471-4159.2010.07135.x

Brambilla, R., Bracchi-Ricard, V., Hu, W.-H., Frydel, B., Bramwell, A., Karmally, S., … Bethea, J. R. (2005). Inhibition of astroglial nuclear factor kappaB reduces inflammation and improves functional recovery after spinal cord injury. *The Journal of Experimental Medicine*, *202*(1), 145–156. https://doi.org/10.1084/jem.20041918

Brix, B., Mesters, J. R., Pellerin, L., & Jöhren, O. (2012). Endothelial cell-derived nitric oxide enhances aerobic glycolysis in astrocytes via HIF-1α-mediated target gene activation. *The Journal of Neuroscience: The Official Journal of the Society for Neuroscience*, *32*(28), 9727–9735. https://doi.org/10.1523/JNEUROSCI.0879-12.2012

Campbell, J. M., Stephenson, M. D., de Courten, B., Chapman, I., Bellman, S. M., & Aromataris, E. (2018). Metformin use associated with reduced risk of dementia in patients with diabetes: A systematic review and meta-analysis. *Journal of Alzheimer's Disease: JAD*, *65*(4), 1225–1236. https://doi.org/10.3233/JAD-180263

Caslin, H. L., Taruselli, M. T., Haque, T., Pondicherry, N., Baldwin, E. A., Barnstein, B. O., & Ryan, J. J. (2018). Inhibiting glycolysis and ATP production attenuates IL-33-mediated mast cell function and peritonitis. *Frontiers in Immunology*, *9*(3026), 1–13. https://doi.org/10.3389/fimmu.2018.03026

Douglass, J., Dorfman, M., Fasnacht, R., Shaffer, L., & Thaler, J. (2017). Astrocyte IKKβ/NF-κB signaling is required for diet-induced obesity and hypothalamic inflammation. *Molecular Metabolism*, *6*(4), 366–373. https://doi.org/10.1016/j.molmet.2017.01.010

Fujioka, S., Schmidt, C., Sclabas, G. M., Li, Z., Pelicano, H., Peng, B., … Chiao, P. J. (2004). Stabilization of p53 is a novel mechanism for proapoptotic function of NF-κB. *Journal of Biological Chemistry*, *279* (26), 27549–27559. https://doi.org/10.1074/jbc.M313435200

Gao, X., Wang, H., Yang, J. J., Liu, X., & Liu, Z.-R. (2012). Pyruvate kinase M2 regulates gene transcription by acting as a protein kinase. *Molecular Cell*, *45*(5), 598–609. https://doi.org/10.1016/j.molcel.2012.01.001

Gavillet, M., Allaman, I., & Magistretti, P. J. (2008). Modulation of astrocytic metabolic phenotype by proinflammatory cytokines. *Glia*, *56*(9), 975–989. https://doi.org/10.1002/glia.20671

Goetzman, E. S., & Prochownik, E. V. (2018). The role for Myc in coordinating glycolysis, oxidative phosphorylation, glutaminolysis, and fatty acid metabolism in normal and neoplastic tissues. *Frontiers in Endocrinology*, *9*(126), 1–25. https://doi.org/10.3389/fendo.2018.00129

Goldfine, A. B., Fonseca, V., Jablonski, K. A., Pyle, L., Staten, M. A., Shoelson, S. E., & Team, T.-T. D. S. (2010). The effects of salsalate on glycemic control in patients with type 2 diabetes: A randomized trial. *Annals of Internal Medicine*, *152*(6), 346–357. https://doi.org/10.7326/0003-4819-152-6-201003160-00004

Goldfine, A. B., Silver, R., Aldhahi, W., Cai, D., Tatro, E., Lee, J., & Shoelson, S. E. (2008). Use of salsalate to target inflammation in the treatment of insulin resistance and type 2 diabetes. *Clinical and Translational Science*, *1*(1), 36–43. https://doi.org/10.1111/j.1752-8062.2008.00026.x

Hertz, L., & Hertz, E. (2003). Cataplerotic TCA cycle flux determined as glutamate-sustained oxygen consumption in primary cultures of astrocytes. *Neurochemistry International*, *43*, 355–361. https://doi.org/10.1016/S0197-0186(03)00022-6

Jiang, T., & Cadenas, E. (2014). Astrocytic metabolic and inflammatory changes as a function of age. *Aging Cell*, *13*(6), 1059–1067. https://doi.org/10.1111/acel.12268

Johnson, R. F., & Perkins, N. D. (2012). Nuclear factor-κB, p53, and mitochondria: Regulation of cellular metabolism and the Warburg effect. *Trends in Biochemical Sciences*, *37*(8), 317–324. https://doi.org/10.1016/j.tibs.2012.04.002

Koenig, A. M., Mechanic-Hamilton, D., Xie, S. X., Combs, M. F., Cappola, A. R., Xie, L., … Arnold, S. E. (2017). Effects of the insulin sensitizer metformin in Alzheimer disease: Pilot data from a randomized placebo-controlled crossover study. *Alzheimer Disease and Associated Disorders*, *31*(2), 107–113. https://doi.org/10.1097/WAD.0000000000000202

La Rosa, F. A., Pierce, J. W., & Sonenshein, G. E. (1994). Differential regulation of the c-myc oncogene promoter by the NF-kappa B rel family of transcription factors. *Molecular and Cellular Biology*, *14*(2), 1039–1044. https://doi.org/10.1128/mcb.14.2.1039

Lee, Y. S., Wollam, J., & Olefsky, J. M. (2018). An integrated view of immunometabolism. *Cell*, *172*(1), 22–40. https://doi.org/10.1016/j.cell.2017.12.025

Liddelow, S. A., Guttenplan, K. A., Clarke, L. E., Bennett, F. C., Bohlen, C. J., Schirmer, L., … Barres, B. A. (2017). Neurotoxic reactive astrocytes are induced by activated microglia. *Nature*, *541*(7638), 481–487. https://doi.org/10.1038/nature21029

Londhe, P., Yu, P. Y., Ijiri, Y., Ladner, K. J., Fenger, J. M., London, C., … Guttridge, D. C. (2018). Classical NF-κB metabolically reprograms sarcoma cells through regulation of hexokinase 2. *Frontiers in Oncology*, *8* (104). https://doi.org/10.3389/fonc.2018.00104

Mauro, C., Leow, S. C., Anso, E., Rocha, S., Thotakura, A. K., Tornatore, L., … Franzoso, G. (2011). NF-κB controls energy homeostasis and metabolic adaptation by upregulating mitochondrial respiration. *Nature Cell Biology*, *13*(10), 1272–1279. https://doi.org/10.1038/ncb2324

McGettrick, A. F., & O'Neill, L. A. J. (2013). How metabolism generates signals during innate immunity and inflammation. *Journal of Biological Chemistry*, *288*(32), 22893–22898. https://doi.org/10.1074/jbc.R113.486464

Meares, G. P., Qin, H., Liu, Y., Holdbrooks, A. T., & Benveniste, E. N. (2013). AMP-activated protein kinase restricts IFN-γ signaling. *Journal of Immunology*, *190*(1), 372–380. https://doi.org/10.4049/jimmunol.1202390

Menk, A. V., Scharping, N. E., Moreci, R. S., Zeng, X., Guy, C., Salvatore, S., … Delgoffe, G. M. (2018). Early TCR signaling induces rapid aerobic glycolysis enabling distinct acute T cell effector functions. *Cell Reports*, *22*(6), 1509–1521. https://doi.org/10.1016/j.celrep.2018.01.040

Nan, J., Du, Y., Chen, X., Bai, Q., Wang, Y., Zhang, X., … Yang, J. (2014). TPCA-1 is a direct dual inhibitor of STAT3 and NF-κB and regresses mutant EGFR-associated human non-small cell lung cancers. *Molecular Cancer Therapeutics*, *13*(3), 617–629. https://doi.org/10.1158/1535-7163.Mct-13-0464

Nissen, J. D., Pajęcka, K., Stridh, M. H., Skytt, D. M., & Waagepetersen, H. S. (2015). Dysfunctional TCA-cycle metabolism in glutamate dehydrogenase deficient astrocytes. *Glia*, *60*(12), 2313–2326. https://doi.org/10.1002/glia.22895

Norata, G. D., Caligiuri, G., Chavakis, T., Matarese, G., Netea, M. G., Nicoletti, A., … Marelli-Berg, F. M. (2015). The cellular and molecular basis of translational immunometabolism. *Immunity*, *43*(3), 421–434. https://doi.org/10.1016/j.immuni.2015.08.023

O'Neill, L. A. J., Kishton, R. J., & Rathmell, J. (2016). A guide to immunometabolism for immunologists. *Nature Reviews Immunology*, *16*(9), 553–565. https://doi.org/10.1038/nri.2016.70

Poli, V., & Camporeale, A. (2015). STAT3-mediated metabolic reprograming in cellular transformation and implications for drug resistance. *Frontiers in Oncology*, *5*(121), 1–9. https://doi.org/10.3389/fonc.2015.00121

Russell, D. G., Huang, L., & VanderVen, B. C. (2019). Immunometabolism at the interface between macrophages and pathogens. *Nature Reviews Immunology*, *19*(5), 291–304. https://doi.org/10.1038/s41577-019-0124-9

Schildge, S., Bohrer, C., Beck, K., & Schachtrup, C. (2013). Isolation and culture of mouse cortical astrocytes. *Journal of Visualized Experiments: JoVE*, *71*, 50079. https://doi.org/10.3791/50079

Schindelin, J., Arganda-Carreras, I., Frise, E., Kaynig, V., Longair, M., Pietzsch, T., … Cardona, A. (2012). Fiji: An open-source platform for biological-image analysis. *Nature Methods*, *9*, 676–682. https://doi.org/10.1038/nmeth.2019

Schneider, C. A., Rasband, W. S., & Eliceiri, K. W. (2012). NIH image to ImageJ: 25 years of image analysis. *Nature Methods*, *9*, 671–675. https://doi.org/10.1038/nmeth.2089

Schwartzenberg-Bar-Yoseph, F., Armoni, M., & Karnieli, E. (2004). The tumor suppressor p53 down-regulates glucose transporters GLUT1 and GLUT4 gene expression. *Cancer Research*, *64*(7), 2627–2633. https://doi.org/10.1158/0008-5472.Can-03-0846

Sharma, J. N., Al-Omran, A., & Parvathy, S. S. (2007). Role of nitric oxide in inflammatory diseases. *Inflammopharmacology*, *15*(6), 252–259. https://doi.org/10.1007/s10787-007-0013-x

Singer, K., Cheng, W.-C., Kreutz, M., Ho, P.-C., & Siska, P. J. (2018). Immunometabolism in cancer at a glance. *Disease Models & Mechanisms*, *11* (8), 1–10. https://doi.org/10.1242/dmm.034272

Sofroniew, M. V., & Vinters, H. V. (2010). Astrocytes: Biology and pathology. *Acta Neuropathologica*, *119*(1), 7–35. https://doi.org/10.1007/s00401-009-0619-8

Sommermann, T. G., O'Neill, K., Plas, D. R., & Cahir-McFarland, E. (2011). IKKβ and NF-κB transcription govern lymphoma cell survival through AKT-induced plasma membrane trafficking of GLUT1. *Cancer Research*, *71*(23), 1–10. https://doi.org/10.1158/0008-5472.Can-11-1715

Viola, A., Munari, F., Sánchez-Rodríguez, R., Scolaro, T., & Castegna, A. (2019). The metabolic signature of macrophage responses. *Frontiers in Immunology*, *10*, 1462. https://doi.org/10.3389/fimmu.2019.01462

Vlachaki Walker, J. M., Robb, J. L., Cruz, A. M., Malhi, A., Weightman Potter, P. G., Ashford, M. L. J., … Beall, C. (2017). AMP-activated protein kinase (AMPK) activator A-769662 increases intracellular calcium and ATP release from astrocytes in an AMPK-independent manner. *Diabetes, Obesity and Metabolism*, *19*(7), 997–1005. https://doi.org/10.1111/dom.12912

Wang, F., Zhang, S., Vuckovic, I., Jeon, R., Lerman, A., Folmes, C. D., … Herrmann, J. (2018). Glycolytic stimulation is not a requirement for M2 macrophage differentiation. *Cell Metabolism*, *28*(3), 463–475.e4. https://doi.org/10.1016/j.cmet.2018.08.012

Williams, N. C., O'Neill, L. A. J., & O'Neill, L. A. J. (2018). A role for the Krebs cycle intermediate citrate in metabolic reprogramming in innate immunity and inflammation. *Frontiers in Immunology*, *9*(141), 141. https://doi.org/10.3389/fimmu.2018.00141

Zamanian, J. L., Xu, L., Foo, L. C., Nouri, N., Zhou, L., Giffard, R. G., & Barres, B. A. (2012). Genomic analysis of reactive astrogliosis. *The Journal of Neuroscience: The Official Journal of the Society for Neuroscience*, *32*(18), 6391–6410. https://doi.org/10.1523/JNEUROSCI.6221-11.2012

## SUPPORTING INFORMATION

Additional supporting information may be found online in the Supporting Information section at the end of this article.

**How to cite this article:** Robb JL, Hammad NA, Weightman Potter PG, Chilton JK, Beall C, Ellacott KLJ. The metabolic response to inflammation in astrocytes is regulated by nuclear factor-kappa B signaling. *Glia*. 2020;68:2246–2263. https://doi.org/10.1002/glia.23835